Coriolis force-driven instabilities in stratified miscible layers on a rotationally actuated microfluidic platform

Saunak Sengupta,[1] Sukhendu Ghosh,[2,3] Sandeep Saha,[4] and Suman Chakraborty[1]
[1]*Department of Mechanical Engineering, Indian Institute of Technology, Kharagpur- 721302, India*
[2]*Department of Mathematics, Presidency University, Kolkata-700073, India*
[3]*Department of Mathematics, Indian Institute of Technology, Jodhpur-342037, India*
[4]*Department of Aerospace Engineering, Indian Institute of Technology, Kharagpur-721302, India*

(Received 28 June 2019; published 13 November 2019)

Stability analysis of stratified multiphase flow for a spanwise system of rotation plays a pivotal role in micromixing and micromachines. In several such systems, centrifugal actuation is the driving force, which creates a pressure gradient in a rotating channel and Coriolis force enhances mixing in a short span by destabilizing the flow. Here, we focus on the impact of the Coriolis force on a rotating two-fluid flow through a microchannel, which is miscible in nature, having small viscosity difference and thereby forming a thin diffusive interface between fluids due to viscosity stratification. Modal stability analysis is used to estimate the critical flow parameters which are, in turn, responsible for regulating the instability mechanism for different viscosity contrasts and mixed layer thicknesses. Usually, viscosity stratified flow with respect to streamwise disturbance becomes more unstable for a thinner mixed layer. On the contrary, our numerical computation confirms a completely discrepant scenario by considering Coriolis force-driven instability of a miscible flow system on account of spanwise disturbances. Possible physical mechanisms for the same are discussed in terms of base flow pattern and the energy fluctuation between the perturbed and base flow. Comparison of three-dimensional disturbances of the flow field, in both clockwise and anticlockwise directions (for two different viscosity ratios), is executed to provide an insight into the dynamics of the flow system. Distributions of the velocity perturbations display a critical bonding between the vortices near and away from the mixed layer. These vortices are, in turn, responsible for the variation in instability mechanism with respect to different viscosity ratios and rotational directions.

DOI: 10.1103/PhysRevFluids.4.113902

I. INTRODUCTION

Hydrodynamic stability of stratified flow (variation in density, viscosity, concentration, etc., or a combination thereof) has drawn the attention of numerous researchers due to various industrial, chemical, biological, and geophysical applications (which include lubrication, drag reduction, manufacture of conjugated fibers, polymer melt, co-extrusion processes, filtration processes, etc.). In recent years, bounded or semibounded flows (with or without stratification) in a rotating platform have been receiving progressively increasing attention because of its potential role in portable medical diagnostic devices. A proper understanding of instability mechanism in such flows is critical to several other practical applications, [1] ranging from pumps, vacuum cleaners, jet engines, etc., on one side of the spectrum to the microfluidic mixer on the other side.

In a wide variety of fluid flows, the viscosity can vary with space, time, or both, resulting in viscosity stratification, which can have a significant impact on flow instability [2–6]. Such a viscosity stratification can be achieved by various means, for example (a) considering two or more immiscible fluids which are in contact with each other (where slope of velocity profile is

discontinuous), (b) including temperature or concentration difference between the fluids which can create a new thin diffusive layer, and (c) deploying a non-Newtonian fluid, where the effective viscosity is a nonlinear function of space or imposed shear rate [7,8].

Investigations on nonrotating viscosity stratified flow have often provided strikingly contradictory results concerning their possible roles on stabilization or destabilization. Yih [9] was the first researcher to explore the instability of multilayer viscosity stratified flow. He focused on a long-wave perturbation analysis and arrived at the following significant conclusion: both plane Poiseuillle flow and plane Couette flow can be unstable for arbitrarily small Reynolds numbers due to viscosity stratification. Therefore, the multilayer flow has been a topic of many other theoretical investigations [10–15] and different instability mechanisms have been discussed. Based on the aforementioned studies and observations, it can be concluded that to achieve a linearly stable flow, the fluid of relatively lesser viscosity must be placed close to a wall.

Several earlier studies have reported instabilities in viscosity stratified flows due to the variation of either temperature or concentration by considering the formation of miscible layer flow inside a channel [3,13,15–18] or over an inclined plane [19–24]. Correspondingly, Wall and Wilson [17] explored the temperature dependent viscosity variation on a wall-bounded flow and showed that the effect of Péclet number has negligible influence on the stability (the difference in their case in calculating the critical Reynolds number for Péclet number 0 and 10^5 is less than 2%). Investigation on Stokes flow (low Reynolds number flow) through a channel of elastic liquids (an Oldroyd-B fluid) having continuously stratified constitutive properties has governed the instability mechanism due to the rapid normal stress variation [25]. Various authors, notably Sahu and Matar [26], considered the influence of viscous heating in different flows. They have shown a decrease in critical Reynolds number as the viscous heating increases [27–29]. Tan and Homsy [30] explored the case of stability of rectilinear displacement process in a porous medium by assuming a quasi-steady-state approximation of the base state profile evolving slowly with respect to growth of the disturbances and comparing the same with the uniform base state velocity and a dispersive time dependent concentration profile. A similar study was there after reported by Tan and Homsy [31] for radial source flow in a porous medium. Despite the absence of characteristic time or length scale available for the system, it was shown that the stability of the system depends on a similarity variable depending on Péclet number. Salin used an acoustic technique profile analysis to study the growth rate for three-dimensional viscous fingers inside a porous medium [32]. Their experimental results suggested an instability parameter that is liable to capture the essential features of viscous fingering depending on viscosity ratio, flow rate and the nature of the porous medium.

Miscible multiphase flows with confined geometries are special kinds of stratified flows which reveal many interesting facets of instability [13,15,18,33,34]. At very low miscibility, stratified flows exhibit instability characteristics similar to immiscible fluids. Investigations further suggest that a decrease in viscosity near the wall increases the critical Reynolds number significantly in some situations [15]. However, such a reduction in viscosity can also bring about the opposite scenario, i.e., instability at extremely low Reynolds numbers [35]. Ranganathan and Govindarajan [15] and subsequently by Malik and Hooper [13] showed linear stability and energy growth of a viscosity stratified flow, by replacing liquid-liquid interface with a miscible layer of variable viscosity.

Ern *et al.* [33] and Sahu *et al.* [34] have discussed the influence of diffusion and mixed layer thickness on Couette type miscible two-fluid flow with a high degree of viscous stratification. They observed the growth rate for the flow which shows a nonmonotonic behavior with respect to diffusion and such flows with intermediate values of Péclet number is more unstable for a thinner mixed layer. Govindarajan and coworkers [15,18] deliberated on the impact of a thin continuous stratified layer created by miscibility of two fluids with different viscosities and examined the effect of slow diffusion. They identified a new mode of instability, which is very sensitive to the diffusion and associated with the overlapping of a critical layer and viscosity stratified layer. Thereafter, Talon and Meiburg [36] considered stability analysis on similar kind channel flow in the Stokes flow regime and demonstrated that instabilities develop due to the diffusion between the layers. However, at large wave numbers, the onset of instability takes place at a highly viscous region

(in the core of the pipe). In the recent past, the work of Govindarajan [18] was extended by Ghosh *et al.* [24] to assess the effects of wall velocity slip on the instabilities of miscible viscosity stratified flow. It was shown that the flow system could either be stabilized or destabilized by designing the walls of the channel as hydrophobic surfaces, modeled by the Navier-slip boundary condition.

In the context of microfluidics, the viscous force commonly dominates over inertial force and mixing due to turbulence driven by inertia is not common. However, the possibility of enhanced mixing by employing instabilities in viscosity stratified layers has been explored as an alternative approach [37–43]. In the case of centrifugal microfluidics, rotational effects can bring about inertial perturbations, whereas the possibility of enhanced mixing can be probed by triggering the instability mechanism [44–47]. Rotationally actuated microfluidic devices, like laboratory on a compact disc (Lab-on-a-CD) platform [48], are inherently adept in generating secondary flow by virtue of the Coriolis force [49,50]. Adding to this, in the rotationally actuated microfluidic device, viscosity stratified miscible layers can depict many interesting flow phenomena. Plane Poiseuille flow, subject to a spanwise perturbation, becomes unstable at very low Reynolds number (at $\leqslant O(100)$) in the presence of rotation [51,52]. The transitional rotating flow patterns were marked by the appearance of the streamwise roll-cell structure, which has been attributed to the Coriolis force [48,53]. Indeed, researchers have suggested that the wavelength of the steady roll-cell instability can be predicted using linear stability theory. The experiments and subsequent theoretical calculations [48] on rotating flows, showing the ratio of Coriolis force to the centrifugal force was the key parameter for achieving mixing in such flows. Investigators also reported that the molecular diffusion dominates at low rotational speed due to the excess of centrifugal force rather than the Coriolis force. Coriolis force-based mixing gets prominence when the rotational speed exceeds an emblematic critical value. The transverse Coriolis force is large enough to set up a secondary flow in such a case [48]. Chakraborty and Chakraborty [54] developed an innovative method of generating microbubbles on a rotationally actuated device in a lab-on-a-compact-disk setup. They have shown the spatiotemporal frequency and size distribution of the generating bubbles by monitoring the rotational speed, for a given channel dimension and fluid-substrate combination. Innovative approaches of generating droplets, liquid threads and diverse configuration of liquid filled entities are reported in the literature [55–62]. Recent work on Lab-On-a-CD-based platform [63] for a simple "Y"-shaped microchannel depicted generation of simple to complex-shaped liquid objects by maneuvering the Coriolis force for a two-fluid system with different viscosities. These investigators established a qualitative relationship between the droplet generation frequency and droplet sizes by varying the rotation speed. The underlying mechanism of generating droplets of simple and complex serpentine threads was achieved by exploiting the Coriolis force. The study of deformation characteristics of red blood cells (RBC or erythrocytes) on a rotating compact disk platform reveals the interplay between hemoglobin content and deformability of RBCs in centrifugally actuated microfluidic device [64]. The study opens up the fact that the deformation of RBC follows a very similar trend of principal stress distribution in a radial direction. Numerical simulations of Roy *et al.* [65] indicate that increasing the channel aspect ratio leads to a nonmonotonic behavior in the critical Reynolds number at which, the secondary flow sets in. Unstable modes sourcing from rotation may have a much larger growth rate than that of the so-called two-dimensional spanwise-invariant Tollmien–Schlichting (TS) mode. These observations raise a question as to how the Coriolis force destabilizes the flow and if there is any technique to control the Coriolis force-driven instabilities.

Stability issues governed by Coriolis force on viscosity stratified flows offer with many unanswered questions that can have a far-reaching consequence for future studies. For example, how varying the rotation rate affects the perturbation growth of stratified flow, or how the fluid viscosity ratio influences the stability boundaries for the Coriolis-driven instability, remain unaddressed. Furthermore, how the presence of a miscible layer causes the mixing process in a rotating channel flow also remains unclear. Here, we bring out unique aspects of rotationally driven instabilities in stratified miscible viscous layers. One important concern of the present investigation is to quantitatively pinpoint the onset condition of the primary instability in the subsistence of spanwise disturbances. To address the unanswered questions on viscosity stratified rotating channel flows and

to progress toward a prior theoretical knowledge for designing guidelines of rotational flows, we conduct a modal stability analysis for the same.

The article is organized as follows: In Sec. II, we present the mathematical formulation of the problem and the set of governing equations in the rotating platform. In Sec. III, we address the stability regimes for infinitesimal disturbances (spanwise disturbances) with different viscosity ratios, mixed layer thicknesses, and clockwise or anticlockwise rotations. Influence of three-dimensional disturbances on the considered flow system is elaborated in Sec. IV. Finally, the concluding section contains a complete summary of the current study.

II. THEORETICAL FORMULATION

The stability property of fluid flows having an interface with zero thickness is substantially different from those of the miscible flow. The difference is mainly because of the finite thickness mixed/interface layer, which occurs by a slow diffusion process and causes a smooth density and/or viscosity, concentration distribution instead of jump discontinuity. The above-mentioned approach was first introduced by Ranganathan and Govindarajan (2001) [15] and subsequently by Malik and Hooper (2005) [13], to the best of our knowledge. Behavior of such systems, hallmarked by flow of two fluids of different viscosities and separated by a *frozen* miscible layer, is significantly different from interface-dominated stratified flows. The most delicate underlying physical issue stems from the fact that the flow exhibits significant alterations in stability properties when the critical layer of disturbances overlaps with the miscible layer [15]. This information can be used for controlling flow systems. The growth of the miscible layer in streamwise direction is, however, ignored because of very slow diffusion. This is exact when the Péclet number of the flow (Pe $= U_0 D/\kappa$,where U_0 is maximum velocity of the flow through a channel, D is the half channel width, and κ is appropriate diffusivity) is very high (in the limit of zero diffusion) [15,66]. A real flow would not necessarily have a very small Péclet number, especially for two distinct fluids and when viscosity stratification is due to concentration/temperature gradient. However, Wall and Wilson [17] showed that for the case of stability of stratified flows, the value of the critical Reynolds number is highly insensitive to Pe. We have assumed that the effect of the Péclet number has negligible influence on the instability, and the viscosity profile is independent of the concentration variation [13]. Also, we assume that the temporal growth rate of the disturbance is much faster than the diffusion rate (which is indeed true for the flow under investigation) of the base flow, so that the assumption of the steady base state is valid [67]. In summary, the disturbance wavelength in spanwise direction for the considered channel flow with the system of rotation is much shorter than the downstream length scale over which the mixed layer thickness grows, so that it is justifiable to use a locally constant thickness approximation [2,3]. In the present study, we consider the modal linear stability of a laminar rotating three-dimensional pressure-driven channel flow of two Newtonian, miscible, incompressible fluids. Study of this type of system is particularly appealing as it concerns a simple rotating shear type flow, which offers both stable and unstable regions depending on different ranges of parameters. Here, the two fluids are having the same density ρ but with different viscosities. A mixed layer with continuously varying viscosity separates the fluid layers with constant viscosity. However, to ignore the complexity of the analysis, a frozen type mixed layer is considered and such an approximation is also used by many previous investigators [13,15,23,36,67].

We emphasize that a rotational system with spanwise disturbance, where Coriolis force is required to drive the instability mechanism, molecular diffusion may play an important role on the instability mechanism for a flow with finite width interfacial region. However, a parallel flow appears to be a good assumption and avoids the complication of analyzing instability behavior for the miscible flows in the parameter regime we are working on. The flow is not necessarily symmetric about the centerline of the channel (see Fig. 1). A Cartesian coordinate system is chosen for the present analysis, where x and y axes are, respectively, the mean flow and wall normal directions. The entire system is rotating with an angular velocity Ω about the z axis whose direction follows the left-hand rule. The walls of the channel are located at the positions $y = \pm D$. Two fluids with

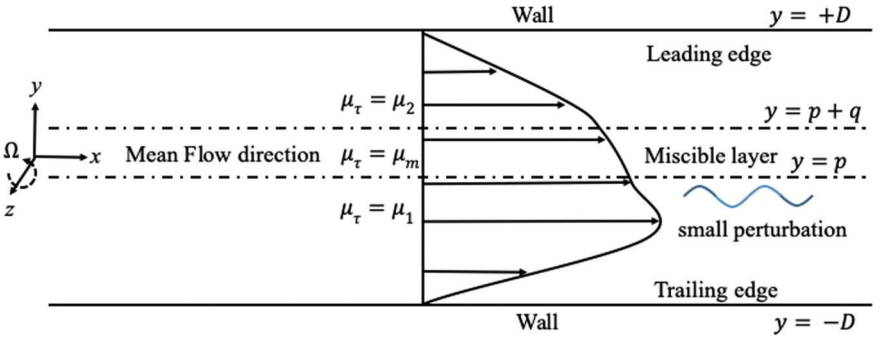

FIG. 1. Schematic of the flow system considered. The entire system is rotating about the z axis, which is taken to be perpendicular to the plane of the paper.

viscosity μ_1 and μ_2 occupy the regions $-D \leqslant y \leqslant p$ and $p+q \leqslant y \leqslant +D$, respectively. The thin diffusive layer (between two constant viscosity fluid layers), referred to as the mixed layer, occupies the region $p \leqslant y \leqslant p+q$, where two fluids are mixed up and a local smooth viscosity stratification is created. In this study, we have fixed the starting point of the mixed layer at $p = 0.0$ for all numerical results.

A. Governing equations

The governing differential equations for the mass and momentum conservation of the above rotating anatomy are (in dimensional form),

$$\nabla.\vec{u}_\tau = 0, \tag{1}$$

$$\frac{\partial \vec{u}_\tau}{\partial t} + (\vec{u}_\tau.\nabla)\vec{u}_\tau = -\frac{1}{\rho}\nabla p_\tau + \nabla.\bar{\tau}_\tau - \frac{2}{\rho}(\vec{\Omega} \times \vec{u}_\tau), \tag{2}$$

$$p_\tau = \bar{p}_\tau - \rho\Omega^2(x^2 + y^2), \tag{3}$$

where $\tau = u, m, l$ pertain to the upper, mixed, and the lower layer, respectively. The variables $\vec{u}_\tau$, p_τ, and $\bar{p}_\tau$ are, respectively, the velocity vector, modified pressure, and pressure without rotation of the flow system. The viscous stress of the flow system is defined as $\bar{\tau}_\tau = \frac{\mu_\tau(y)}{\rho}((\nabla\vec{u}_\tau) + (\nabla\vec{u}_\tau)^T)$; $\mu_\tau(y)$ represents dynamic viscosity of each layer. The last term in the momentum equation originates from the system rotation ($\vec{\Omega} = \Omega\hat{k}$, $\hat{k}$ is the unit vector along the z axis), due to the presence of the Coriolis force. The governing equations, as well as the flow variables, are nondimensionalized by using the half channel width D as length scale, the maximum velocity of the flow U_0 as velocity scale [13], and the viscosity of the lower layer μ_1. The dimensionless viscosity for each layer reads as

$$\mu_\tau(y) = \begin{cases} 1.0, & -1 \leqslant y \leqslant p \quad (\text{for } \tau = l), \\ \mu_m(y), & p \leqslant y \leqslant p+q \quad (\text{for } \tau = m), \\ r, & p+q \leqslant y \leqslant 1 \quad (\text{for } \tau = u), \end{cases} \tag{4}$$

where $r = \mu_2/\mu_1$ is the viscosity ratio of the two fluids. The dimensionless viscosity $\mu_\tau(y)$ is chosen in such way so that the viscosity function and its first, second derivatives are continuous at the edge points of the miscible layer (i.e., at $y = p$ and $y = p+q$). This particular consideration can ensure the continuity in the linearized disturbance equation [13,18]. We have taken the viscosity of the miscible layer to be a fifth-order polynomial with appropriate coefficients and given by Malik and Hooper (2005) [13],

$$\mu_m(y) = s_5y^5 + s_4y^4 + s_3y^3 + s_2y^2 + s_1y + s_0, \tag{5}$$

where the coefficients s_0, s_1, s_2, s_3, s_4, and s_5 are defined as follows:

$$s_0 = 1 - \frac{p^3(r-1)}{q^5}(6p^2 + 15pq + 10q^2); \quad s_1 = \frac{30p^2(r-1)}{q^5}(p^2 + 2pq + q^2);$$
$$s_2 = -\frac{30p(r-1)}{q^5}(2p^2 + 3pq + q^2); \quad s_3 = \frac{10(r-1)}{q^5}(6p^2 + 6pq + q^2);$$
$$s_4 = -\frac{15(r-1)}{q^5}(2p + q); \quad s_5 = \frac{6(r-1)}{q^5}.$$

Equations (4) and (5) are reminiscent of one kind of approximate viscosity profile which confirms the continuity of the profile as well as certain order of derivatives. One can also use other continuous differentiable functions like error function or hyperbolic function. Since we have followed the work of Malik and Hooper (2005) [13] and Govindarajan [18] as the main references for the current work, we have adhered to their formulation.

The unidirectional steady and fully developed basic flow is derived from the following dimensionless equation:

$$\mathrm{Re}\left(\frac{dP}{dx}\right) = \frac{d}{dy}\left(\mu_\tau(y)\frac{dU}{dy}\right). \tag{6}$$

using the no-slip and continuity conditions at the walls and the interfaces, respectively, and the base flow does not get affected by the Coriolis force [47,51,52,68,69]. The derivation is very similar to the derivation of plane Poiseuille flow with a minor difference being viscosity is changing as a function of wall normal direction. The dimensionless typical base velocity profile is derived as [13]

$$U(y) = \begin{cases} \frac{1}{U_0}(-y^2 + (\delta-2)y + (\delta-1)), & -1 \leqslant y \leqslant p \\ \frac{1}{U_0}\int_p^y \left[\frac{-2\bar{y}+(\delta-2)}{\mu(\bar{y})}\right]d\bar{y} + U(p), & p \leqslant y \leqslant p+q, \\ \frac{1}{U_0}\left(\frac{1}{r}\left[-y^2 + (\delta-2)y + b_q\right]\right), & p+q \leqslant y \leqslant +1 \end{cases} \tag{7}$$

where the constant $b_q = rU(p+q) + (p+q)[(p+q) - (\delta-2)]$. Remember that $U(y)$ satisfies zero-velocity at $y = -1$ and U, $\frac{dU}{dy}$ are continuous at the points $y = p$ and $y = p+q$. The value of δ is appropriately estimated by satisfying the no-slip condition at the wall $y = 1$.

B. Generalized Orr-Sommerfeld Squire equations

We focus on the linear stability analysis of the basic/mean flow with respect to three-dimensional small-amplitude disturbances in the form of $\varepsilon(y)\exp[i(\alpha x + \beta z - \omega t)]$. Parameters α, β are the wave numbers of the disturbance in the stream and spanwise directions; $\varepsilon(y)$ and $\omega = \omega_r + i\,\omega_i$ are the amplitude and complex frequency, respectively. The complex phase speed c of the perturbation wave satisfies $\omega = \alpha\, c$ and ω_i is the temporal growth or decay rate. We have used the normal mode formulation of normal velocity ($\tilde{v}$) and vorticity ($\tilde{\eta}$) perturbation given by $\{\tilde{v}, \tilde{\eta}\} = \{v, \eta\}\exp[i(\alpha x + \beta z - \omega t)]$ [70], where

$$\begin{Bmatrix} v \\ \eta \end{Bmatrix} = \begin{cases} \begin{Bmatrix} v_l \\ \eta_l \end{Bmatrix}, & -1 \leqslant y \leqslant p \\ \begin{Bmatrix} v_m \\ \eta_m \end{Bmatrix}, & p \leqslant y \leqslant p+q \\ \begin{Bmatrix} v_u \\ \eta_u \end{Bmatrix}, & p+q \leqslant y \leqslant +1 \end{cases} \tag{8}$$

defines the amplitudes of the velocity and vorticity disturbances at each layer. Perturbation quantities $\{\tilde{v}, \tilde{\eta}\}$ satisfy the generalized Orr-Sommerfeld Squire equation for the variable viscosity

(justification of doing the Squire transformation for the case of rotating channel flow is given in Appendix C) [13,18]. The final equations of disturbances in terms of wall-normal velocity and vorticity yield

$$-i\omega(v''-k^2v)+i\alpha U(v''-k^2v)-U''v$$
$$=\frac{\mu_\tau}{\mathrm{Re}}(v''''-2k^2v''+k^4v)+\frac{2\mu'_\tau}{\mathrm{Re}}(v'''-k^2v')+\frac{2\mu''_\tau}{\mathrm{Re}}(v''+k^2v)-i\beta\mathrm{Ro}\eta \tag{9}$$

$$-i\omega\eta+i\alpha U\eta+i\beta Uv=\frac{\mu_\tau}{\mathrm{Re}}(\eta''-k^2\eta)+\frac{1}{\mathrm{Re}}\eta'\mu'_\tau+i\beta\mathrm{Ro}v, \tag{10}$$

where, $\mathrm{Re}\equiv\frac{\rho DU_0}{\mu_{\mathrm{avg}}}$ and $\mathrm{Ro}\equiv\frac{2D\Omega}{U_0}$ are the Reynolds (μ_{avg} is defined as viscosity averaged in the wall-normal direction [17]) and rotation numbers, respectively, and prime ($'$) denotes differentiation with respect to y (wall-normal direction). In the above equations, μ_τ is the base state viscosity. Moreover, v and η satisfy the no-slip and no-penetration boundary conditions at the channel walls and interface conditions at the edges of the mixed layer,

$$v(-1)=\eta(-1)=v'(-1)=0, \tag{11}$$

$$v(+1)=\eta(+1)=v'(+1)=0, \tag{12}$$

$$v_u(p+q)=v_m(p+q), \tag{13}$$

$$v'_u(p+q)=v'_m(p+q), \tag{14}$$

$$v''_u(p+q)=v''_m(p+q), \tag{15}$$

$$v'''_u(p+q)=v'''_m(p+q), \tag{16}$$

$$v_l(p)=v_m(p), \tag{17}$$

$$v_l{}'(p)=v'_m(p), \tag{18}$$

$$v_l{}''(p)=v''_m(p), \tag{19}$$

$$v_l{}'''(p)=v'''_m(p), \tag{20}$$

$$\eta_u(p+q)=\eta_m(p+q), \tag{21}$$

$$\eta'_u(p+q)=\eta'_m(p+q), \tag{22}$$

$$\eta'_u(p+q)=\eta'_m(p+q), \tag{23}$$

$$\eta_l(p)=\eta_m(p), \tag{24}$$

$$\eta'_l(p)=\eta'_m(p). \tag{25}$$

It is worth mentioning that one can define the Reynolds and rotation number based on flow rate and thereby calculate the average velocity. However, such a definition of Reynolds and rotation numbers does not change the results qualitatively, as shown in Appendix A. The above equations, together with all boundary conditions, are solved numerically using a spectral collocation scheme

described in Schmid and Henningson [71]. The scheme and resulting numerical solutions are described in the next section.

III. NUMERICAL RESULTS AND DISCUSSIONS

The generalized Orr-Sommerfeld Squire equation along with the boundary conditions can be deduced to the following eigenvalue problem after numerical discretization:

$$A\Phi = -i\omega B\Phi, \tag{26}$$

where A and B are 9×9 block matrices and $\Phi = (\Phi_u \Phi_m \Phi_l)^{\mathrm{T}}$ is the eigenfunction corresponding to the eigenvalue ω. A hybrid Chebyshev spectral collocation method is used to solve the above eigenvalue problem. We have considered $n_u + 1$, $n_m + 1$ and $n_l + 1$ numbers of weighting functions in the upper, miscible, and lower layer, respectively, to approximate the eigenfunctions as follows:

$$\Phi_u = \sum_{n=0}^{n_u} a_n T_n(y), \quad \Phi_m = \sum_{n=0}^{n_m} b_n T_n(y), \quad \Phi_l = \sum_{n=0}^{n_l} c_n T_n(y), \tag{27}$$

where $T_n(y)$ represents the Chebyshev polynomial of first kind and a_n, b_n, and c_n are unknown constants. Correspondingly, the Orr-Sommerfeld Squire equation is implemented in each layer at the collocation points [72]:

$$y_j = \cos\left(\frac{\pi j}{M}\right), \quad j = 0, 1, 2, \ldots\ldots M. \tag{28}$$

We take $M = N - 2$ with N equal to n_u, n_m, and n_l in the upper, middle, and lower layers, respectively, giving $2(n_u + n_m + n_l) - 12$ equations. The rest comes from the boundary conditions and thus closing the system. We have used a developed MATLAB code to solve the above-generalized eigenvalue problem. Each sets of parameters described above are varied such that the imaginary part of the eigen value $|\omega_i| \leqslant 10^{-6}$. More details of our numerical analysis and convergence are given in Appendix B.

A. Parametric results

We have elaborated different aspects of instability behavior depending on various parameters with respect to small disturbances for the considered flow system. A wide range of new stability features of three-layer viscosity stratified miscible flow in a channel with a spanwise system of rotation has been discussed. Those include the structure of eigen spectra, neutral stability boundary, eigenfunction behavior, and the role of rotational speed and direction on the flow system. We also have deliberated on the effect of viscosity ratio and layer thickness as well. Eigenvalues are calculated numerically and limiting results are compared with the available results for the nonrotating single-fluid flow [71,73] alongside the rotating single fluid system investigated as by Alfredsson and Persson [52].

Validation of our numerical code is first addressed in Fig. 2(a) by comparing the neutral stability boundary for the single fluid Poiseuille flow in the absence of viscosity contrast ($r = 1.0$) [70,71,73]. The critical Reynolds number, $\mathrm{Re}_{\mathrm{cr}} = 5772.2$ for the onset instability is recovered by our numerical result. We also computed the eigen spectrum (not shown) for the single fluid flow when $\mathrm{Re} = 10\,000$, $\alpha = 1.0$, and $r = 1.0$. The associated most unstable shear mode corresponds to the temporal frequency value $\omega = 0.237526 + 0.0037396i$. Further, we have captured the marginal stability boundary for the rotating single fluid flow from our generalized eigenvalue problem with $\omega = \omega(\alpha, \beta, \mathrm{Re}, \mathrm{Ro}, r, p, q)$. Temporal instability is determined by the condition, the imaginary part of the eigenvalue $\omega_i > 0$ and neutral stability is achieved by satisfying, $\omega_i = 0$. Note that the case of $r = 1.0$ corresponds to a single fluid system with constant viscosity. We have compared our rotating-flow limiting results with Alfredsson and Persson (1989) [52] in Fig. 2(b) and found a very good agreement.

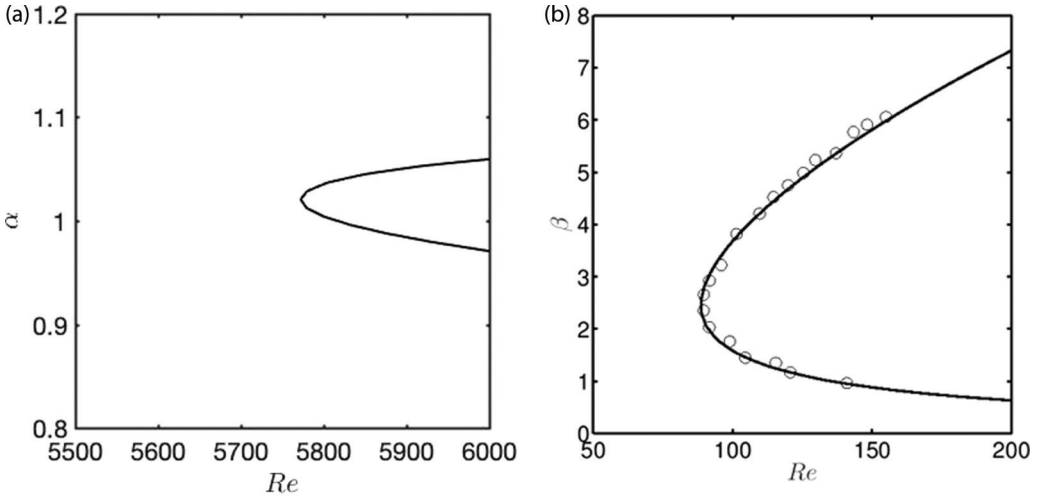

FIG. 2. Neutral stability boundary for plane channel flow, applying single-fluid limit from the two-fluid miscible viscosity stratified Poiseuille type flow: (a) nonrotating single-fluid limit ($r = 1.0, \mathrm{Ro} = 0$) for streamwise disturbances and (b) rotating single-fluid limit with nonzero rotation number ($r = 1.0, \mathrm{Ro} = 0.5$) for spanwise disturbances. Solid line presents our computation result and circles are from Alfredsson and Persson [52] result.

In Fig. 3, we have demonstrated the stability boundaries for two-dimensional disturbances ($\alpha = 0.0$) in $\beta - \mathrm{Re}$ plane for two different viscosity ratios for both anticlockwise and clockwise rotation. In Figs. 3(b) and 3(d), the direction of rotation is clockwise and it is anticlockwise for Figs. 3(a) and 3(c). Notably, clockwise (CW) and anticlockwise (ACW) rotations, respectively, implicate negative and positive rotational number (signs are omitted here). Neutral stability diagrams show distinguishable effects of CW, ACW rotations and in the case of ACW, the system is more unstable (lower the value of critical Reynolds number) for viscosity ratio $r > 1.0$. In the case of rotating single fluid, Lezius and Johnston reported that the critical disturbance mode occurs at the critical Reynolds number $\mathrm{Re}_{\mathrm{cr}} = 88.53$ and the rotation number $\mathrm{Ro} = 0.5$ [51]. Furthermore, an increase in the rotation number stabilizes the system via increasing the $\mathrm{Re}_{\mathrm{cr}}$ value. In congruence with Lezius and Johnston [51], we have found a similar phenomenon for the viscosity stratified rotating channel flow. Both the critical Reynolds number ($\mathrm{Re}_{\mathrm{cr}}$) and the critical rotation number ($\mathrm{Ro}_{\mathrm{cr}}$) vary with respect to the viscosity contrast. Further increase in rotation speed beyond the critical rotation number increases the critical Reynolds number, thereby making the system more stable [74]. However, the scaling of their study is different from the current study. Consequently, the value of $\mathrm{Re}_{\mathrm{cr}}$ and $\mathrm{Ro}_{\mathrm{cr}}$ alter as we change the direction of the rotation (CW or ACW). For a small viscosity variation with $r = 1.2$, our computed critical value of the rotation number ($\mathrm{Ro}_{\mathrm{cr}}$), Reynolds number ($\mathrm{Re}_{\mathrm{cr}}$), and the spanwise wave number (β_{cr}) for anticlockwise rotation are $\mathrm{Ro}_{\mathrm{cr}} = 0.35$, $\mathrm{Re}_{\mathrm{cr}} = 75.38$, and $\beta_{\mathrm{cr}} = 2.56$, respectively.

The relevant parameters are $\mathrm{Ro}_{\mathrm{cr}} = 0.3$, $\mathrm{Re}_{\mathrm{cr}} = 80.023$, and $\beta_{\mathrm{cr}} = 2.3$ for clockwise rotation. Further, increasing the viscosity ratio to $r = 2.0$, a similar trend is observed in the variation of critical values (we found $\mathrm{Re}_{\mathrm{cr}}$ increases to 112.31 but $\mathrm{Ro}_{\mathrm{cr}}$ reduces to 0.28, for anticlockwise rotation). The inclusion of the viscosity variation causes an asymmetry in the base flow which, coupled with the rotational effect, renders the system more susceptible to rotation-induced instability. It is to be noted that for a symmetrical parabolic profile, reversing the direction of rotation does not affect the neutral stability boundary. For the case of the symmetric base velocity profile, the direction of rotation does not affect the neutral stability boundary, because of the fact that the absolute value of wall normal pressure gradient from the central line is same for both the ACW and CW rotation.

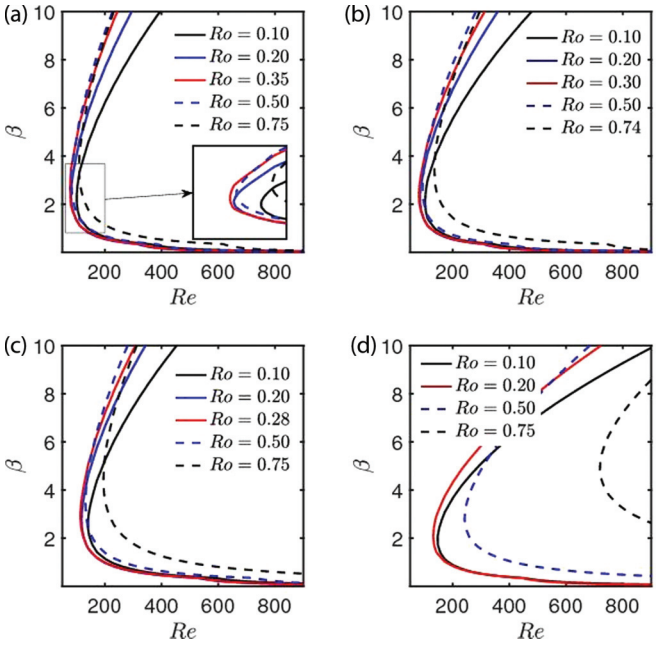

FIG. 3. Neutral stability boundaries for two different viscosity ratios (r): in (a) and (b) panels $r = 1.2$ and in (c) and (d) panels $r = 2.0$. Right and left columns of the figure are for clockwise and anticlockwise rotation, respectively. Critical rotation number ($\mathrm{Ro_{cr}}$) for each configuration are 0.35, 0.30, 0.28, and 0.20 (red lines), respectively.

However, with the viscosity contrast, if a fluid element is considered at the same distance above and below the central line, the absolute value of the wall normal pressure gradient no longer remains to be the same as the case of single-phase flow. Henceforth, $\mathrm{Ro_{cr}}$ adopts a lower value for higher viscosity contrast.

The parameter p represents the location around which the miscible layer starts and q denotes the mixed layer thickness. Both the parameters p and q are very important for this particular type of flow, as they determine the relative mass fluxes of the fluid layers and the skewness of the base velocity profile (the other two critical parameters are the direction of rotation and viscosity ratio). Thus, we aim to examine the influence of mixed layer thickness on the flow instability for both ACW and CW rotation. The neutral stability boundaries for two different viscosity ratios $r = 1.2$ and 2.0 are shown in Fig. 4 for both CW and ACW rotations with variant mixed layer thicknesses. For instance, two different values of the mixed layer thickness are chosen to understand the effect of viscosity stratification and rotational direction on the stability boundaries for a thinner ($q = 0.1$) and a thicker ($q = 0.3$) mixed layer. Earlier investigations on miscible nonrotating flows [3,13,18] indicate that the flow becomes more unstable with respect to two-dimensional streamwise disturbances for a thinner miscible layer. In the inset of Fig. 4(a), for a two-dimensional nonrotating flow with viscosity ratio $r = 1.2$, we have shown that our result to be consistent with the earlier reported results and that the thinner mixed layer is more unstable for streamwise disturbances. It is significant and interesting to note that results for the viscosity-stratified flow with a spanwise system of rotation unveil contrasting physics as compared to what is known earlier in the absence of any kind of rotation. Notably, the present flow system with rotation is more stable for the case of the thinner mixed layer, which is the most significant finding of the current investigation. This observation was not noted in any previous studies, to the best of our knowledge.

In Fig. 4(a), even on varying the thickness of the miscible layer (q), the effect of rotational direction (critical Reynolds number does not change much for ACW or CW rotation) has no

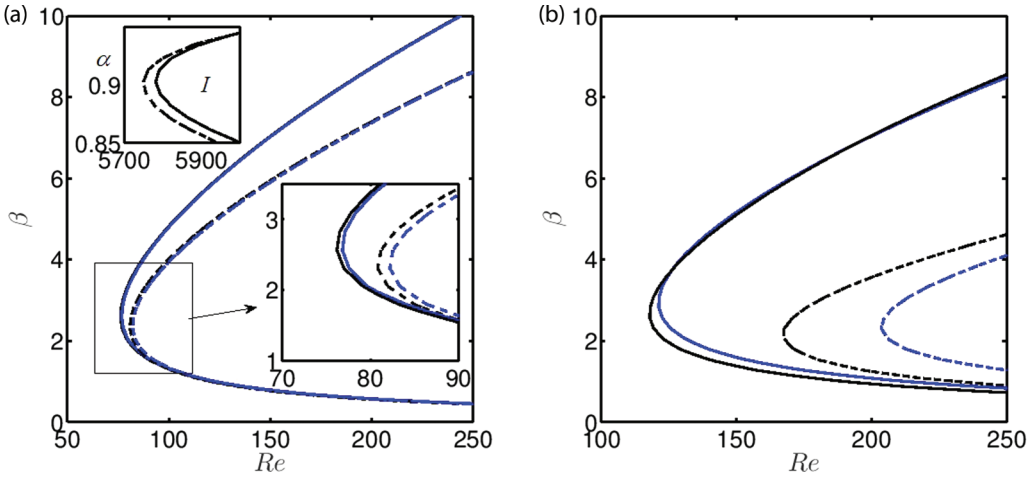

FIG. 4. Neutral stability boundaries for both clockwise (dashed lines) and anticlockwise (solid lines) rotation in conjunction with more viscous fluid is near the upper wall: (a) for $r = 1.2$ and (b) for $r = 2.0$. Black lines are for miscible layer thickness $q = 0.3$ and blue curves are for $q = 0.1$. [In the inset I results for general class of viscosity stratified flow with streamwise disturbance and without any rotation are given (dashed line for mixed layer thickness $q = 0.1$ and solid line for $q = 0.3$)].

significant effect on the neutral stability boundary in the $\beta - \mathrm{Re}$ plane (for $r = 1.2$). However, for thinner mixed layer ($q = 0.1$), the influence of rotational direction is much significant and the flow tends to become more stable at $\beta - \mathrm{Re}$ plane as the viscous force is higher (although $\mathrm{Ro}_{\mathrm{cr}}$ is lesser in the case of CW rotation). The critical Reynolds number remains almost invariant with the variation of layer thickness for ACW rotation when viscosity ratio $r = 1.2$. The reason behind this phenomenon is that the velocity profile does not get affected much by low viscosity contrast. Enhancing the viscosity ratio to $r = 2.0$ [Fig. 4(b)], we see a higher order change in the value of $\mathrm{Re}_{\mathrm{cr}}$ if we switch the mixed layer thickness. This supports the fact that the maximum of base velocity for mixed layer thickness $q = 0.3$ is higher than that of the corresponding $q = 0.1$ (to be noted, we have defined our Reynolds number based on the maximum velocity of the channel). Nevertheless, for clockwise rotation, decreasing the miscible layer thickness makes the flow more stable (for $r > 1.0$). Quite interestingly, the critical value of Reynolds number is achieved at a higher value with an increase of viscosity ratio and it turns out to be a more stable configuration. In Table I, we have enlisted the critical value of rotation number, Reynolds number and spanwise wave number for three different viscosity ratios $r = 0.8$, 1.2, and 2.0, for both clockwise rotation and anticlockwise rotation. It is worth mentioning that, $r = 1.2$, 2.0 suggest the configuration where a fluid with higher

TABLE I. Critical values of the spanwise wave number (β_{cr}), rotation number ($\mathrm{Ro}_{\mathrm{cr}}$), and the Reynolds number ($\mathrm{Re}_{\mathrm{cr}}$). A clockwise rotation signifies negative rotation number but the sign is omitted here. The miscible layer stars at $p = 0.0$ and thickness of the mixed layer considered here is $q = 0.3$.

r	β_{cr}	$\mathrm{Ro}_{\mathrm{cr}}$	$\mathrm{Re}_{\mathrm{cr}}$
0.8	2.41	0.33(ACW)	56.90
0.8	2.76	0.40(CW)	53.44
1.2	2.56	0.35(ACW)	76.38
1.2	2.3	0.30(CW)	81.02
2.0	2.82	0.28(ACW)	112.31
2.0	2.034	0.20(CW)	136.44

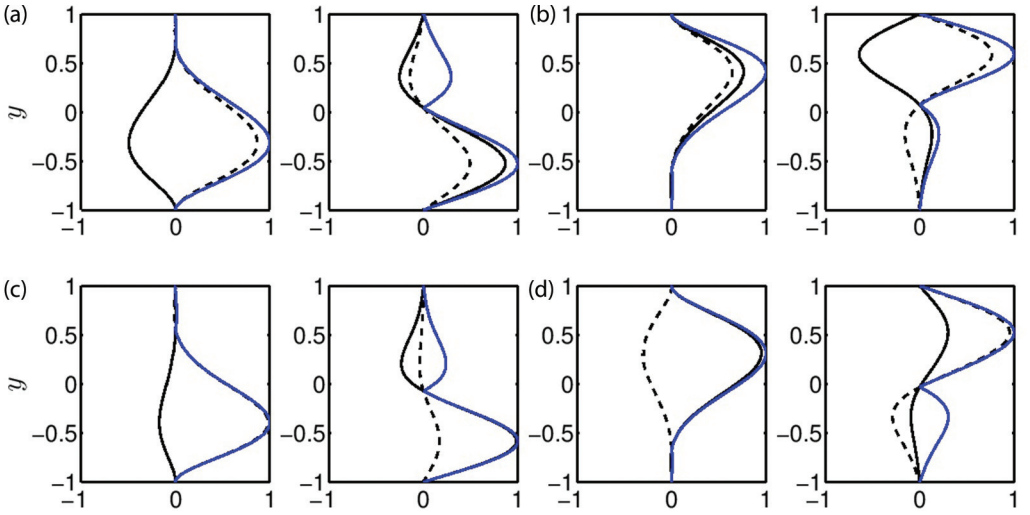

FIG. 5. Typical eigenfunctions for different rotational directions and for two different viscosity ratios $r = 0.8$ [in (a)(ACW rotation), (b) (CW rotation)] and $r = 1.2$ [in (c) (ACW rotation), (d) (CW rotation)]. Left pan and right pan of the sub-figures represent normal velocity and vorticity, respectively. Solid black line for real part and blue line for an absolute value of eigenfunction; dashed line is used for the imaginary part. Critical values of other parameters are used in this figure are given in Table I.

viscosity flows over a low viscous fluid and $r = 0.8$ yields an opposite flow configuration. From the table, it is clear that disturbances are unstable at lower β_{cr}, Ro_{cr} for anticlockwise rotation when $r < 1$ and the same is true for clockwise rotation when $r > 1$.

To give additional physical insight about the evolution of flow instability, the wave amplitude pattern of the wall normal velocity and vorticity (which are nothing but the eigenfunctions) need to be comprehensively assessed. The real, imaginary and the absolute value of the typical eigenfunctions for most excited eigenmode are assembled in Fig. 5 with both CW and ACW rotations. All the eigenfunctions are normalized using supreme norm to make the comparison effective. Disturbances of the spanwise and streamwise velocity components are proportional to the normal vorticity and derivative of normal velocity components, respectively. Figures 5(a), 5(b) and 5(c), 5(d) are drawn for the case $r = 0.8$ and $r = 1.2$, respectively. The critical perturbation of the wall normal velocity attends a maximum value in the bulk of fluid (high viscosity $r = 1.2$**;** less viscosity $r = 0.8$) adjacent to the lower wall for anticlockwise rotation and in the fluid region near to the upper wall (high viscosity $r = 1.2$**;** less viscosity $r = 0.8$) for clockwise rotation. At the same time, the wall normal vorticity of perturbation also attains a global maximum in the same side of that of the wall normal velocity, but it has a local maximum at the opposite side of the mixed layer. The absolute value of amplitude function for wall normal vorticity of perturbations attends a zero value inside the flow domain which suggests the existence of more than one vorticity with different strength within the flow field. The local maximum value in the normal vorticity is appearing near to the miscible layer for anticlockwise rotation, and it is on the other side and away from the mixed layer for clockwise rotation. However, for clockwise rotation, the wall normal velocity and vorticity perturbations attain a positive maximum value around the miscible layer, which supplies extra energy to the disturbances and thus the flow is more unstable in this case. The maximum value attained by the eigenfunctions alters depending on the direction of rotation. Furthermore, the anticlockwise rotation reduces the vorticity-strength of the upper layer (more viscous for $r = 1.2$**;** less viscous for $r = 0.8$) and enhances the vorticity-strength of the lower layer. The above discussion, thus far, provides that paternity of the unstable disturbances depends on the viscosity contrast as well as rotational direction.

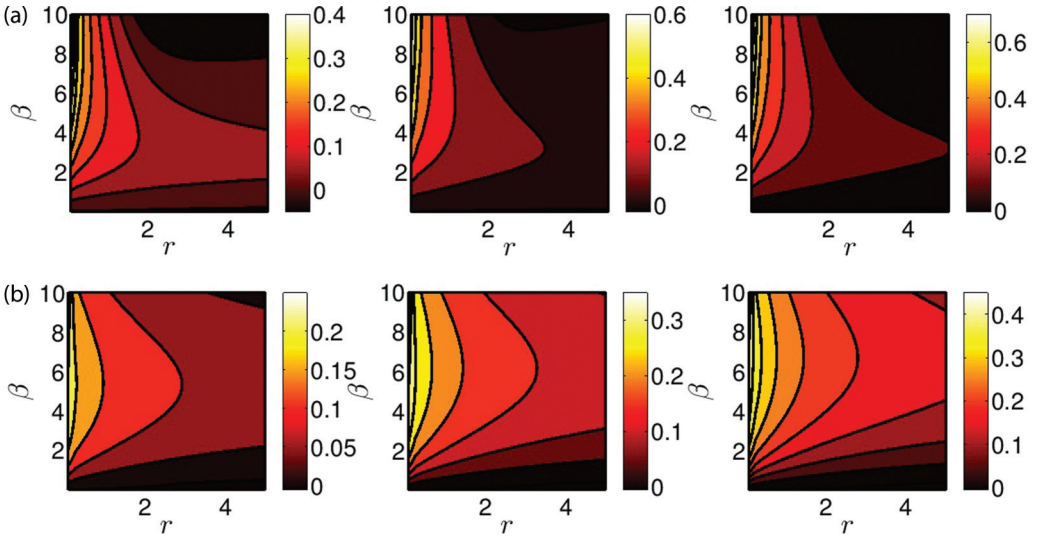

FIG. 6. Contours of maximum growth rate for (a) anticlockwise and (b) clockwise rotation with three different rotation numbers $Ro = 0.1, 0.2, 0.3$. Other parameters are $\alpha = 0.0$, Re $= 995$, $p = 0$, $q = 0.3$.

In Fig. 6, we have focused on the contours of maximum growth rate $\omega_{i,\max}$ by considering all the existing modes across a range of spanwise wave number and viscosity contrast to summarize the instability fashion for a fixed Reynolds number (Re $= 995$). The rotation number is varied to understand the efficiency of the mixing process in the microfluidic system. Rotation number is varied from 0.1 to 0.3, to provide a practical microfluidic perspective. The growth rate for ACW rotation is high as compared to CW rotation and it increases significantly as the rotation number increases from 0.1 to 0.2. However, a further increase in rotation number does not allow the growth rate to increase appreciably. We also noted that the growth rate is much higher for viscosity ratio $r < 1$ and it decreases with the increase in viscosity contrast. In case of longer spanwise wave number (or shorter wavelength), the system tends to be stable for both CW and ACW rotation number.

B. Three-dimensional instability

Our discussion thus far provides two-dimensional (2D) (streamwise wave number is zero) instability behaviors and does not help in dealing with three-dimensional (3D) perturbations. In Fig. 7, the sets of eigenmodes for 3D perturbations are plotted in the complex frequency plane for two different viscosity ratios in conjunction with different rotational directions. The existence of more than one unstable eigenmode is found for the considered set of parameters. Meanwhile, a fundamental query evolves: either the unstable modes are of a similar kind and originate from the same fluid layer, or their properties and origins are different. We have collected the different modes of each layer corresponding to respective Orr-Sommerfeld-Squire operator to identify the origin of unstable eigenmodes. Figures 7(a) and 7(b) confirm that some unstable modes occur due to the presence of the mixed layers (denoted by * symbol). The most unstable mode with maximum growth rate originates from the lower or upper layer, depending on the rotational direction. This mode is achieved with higher temporal growth for viscosity ratio $r = 0.8$, as compared to that for $r = 1.2$. The rotation number and spanwise wave number also play a crucial role in determining the behavior of the spectrum corresponding to three-dimensional disturbances.

Properties of marginal stability boundaries with respect to three-dimensional disturbances are being discussed and compared with the two-dimensional case in Fig. 8 for two different viscosity contrasts, considering both CW and ACW rotation (for rotation number Ro $= 0.2$). The Coriolis

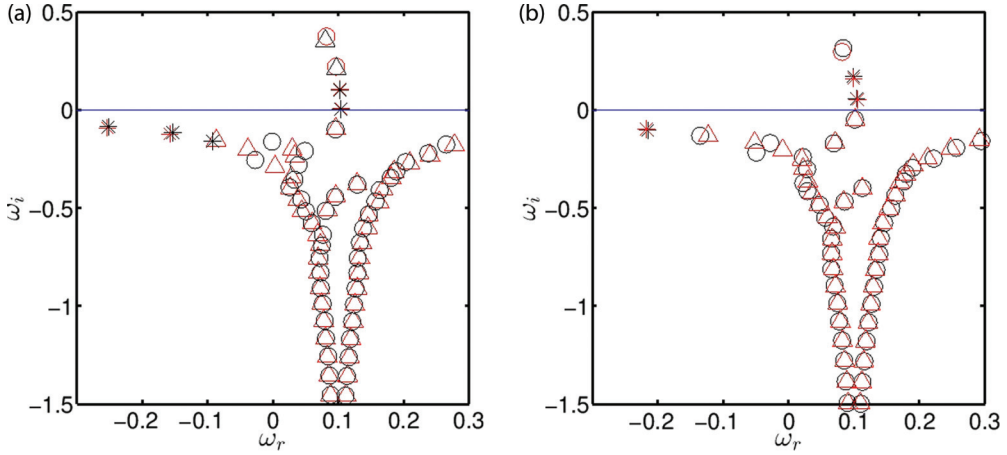

FIG. 7. Eigenspectrum for Re = 995.0, $\alpha = 0.15$, $\beta = 1.0$, Ro = 0.20, with mixed layer thickness $q = 0.3$ and $p = 0.0$: in (a) $r = 0.8$ and in (b) $r = 1.2$. Different symbols are used to distinguish different modes based on their layer of sourcing. Modes, which are coming due to the presence of mixed layer are denoted by $*$ symbol and modes from upper/lower layers are denoted by the symbol o/Δ. Black and red colours suggest anticlockwise and clockwise rotation, respectively.

acceleration gives rise to an opposite directional force, which is normal to the walls in a rotating channel since the basic flow is supposed to be unidirectional and parallel to the walls. This force will be directed toward the leading side of the channel, depending on the direction of rotation. The base flow will have the nearly parabolic type profile (see Fig. 12 for $r = 1.2$), with the largest force being slightly shifted from the center of the channel (thus the profile is not symmetric and center line velocity is not maximum) due to the effect of viscosity stratification. This is coupled with an unstable 'stratification' of the Coriolis force on the leading side, and a stable one on the trailing side. For a fixed viscosity ratio, the direction of the rotation plays a key role. In this kind of system, the

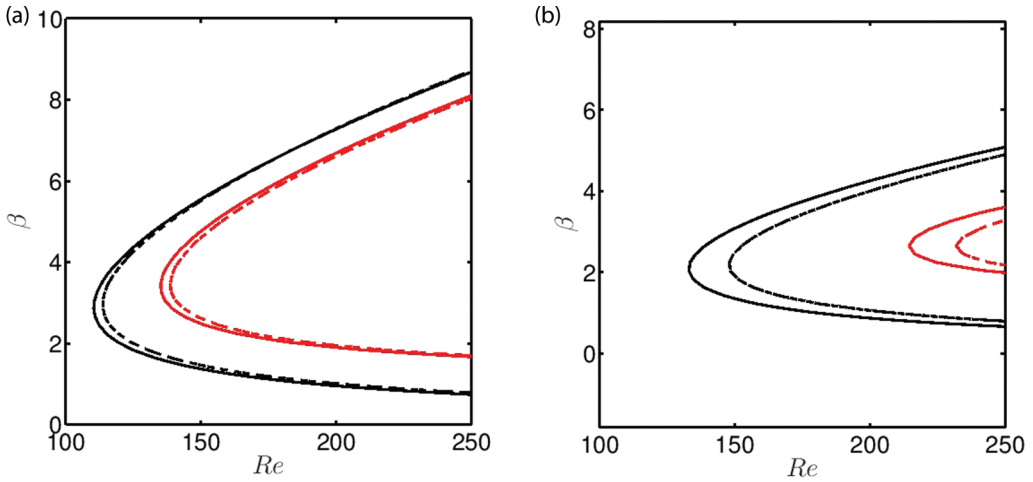

FIG. 8. Marginal stability boundaries for two different viscosity ratios (a) $r = 1.2$ and (b) $r = 2.0$ for two different wave numbers of streamwise disturbances ($\alpha = 0.0$, 1.0). Solid lines are for ACW and dashed lines are for CW rotations. Here, $\alpha = 0.0$ (black lines) corresponds to the two-dimensional disturbance. The other parameters are Ro = 0.20, $q = 0.3$, and $p = 0.0$.

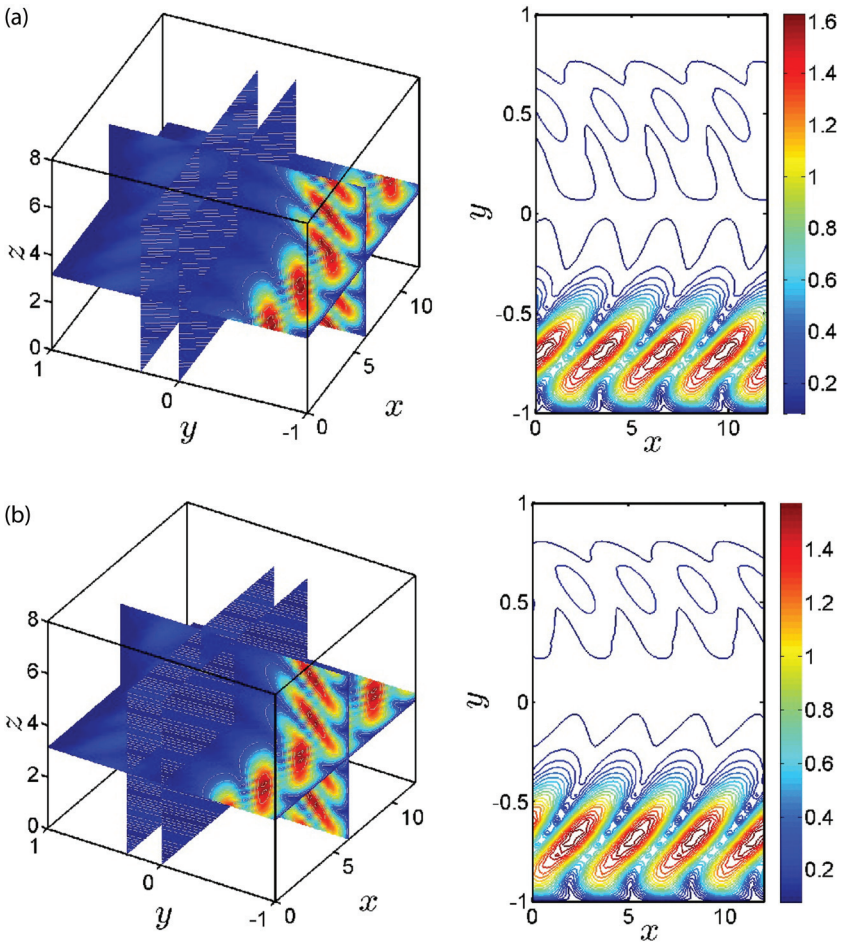

FIG. 9. Iso-contours of velocity field for three-dimensional disturbances with viscosity ratio (a) $r = 1.2$ and (b) $r = 0.8$ (ACWcase : Ro $= 0.2$, Re $= 995, \alpha = 0.15, \beta = 1.0$).The thickness of the miscible layer $q = 0.3$ and miscible layer starts at $p = 0.0$.

leading side is destabilizing and the trailing side is a stabilizing one. For the case of anticlockwise rotation, higher viscous regime falls on the trailing side and the less viscous regime of the flow field is on the leading side, and the reverse is true for the clockwise rotation. As seen in Fig. 3, with anticlockwise rotation the flow becomes more unstable due to the less viscous leading side, which effectively plays an important role in destabilizing the flow. In the clockwise rotation, the flow tends to be more stable due to the effect of higher viscosity in the leading side. The viscosity stratification of the system is effectively suppressing the growth rate of the system as compared to the single fluid rotating system, which is useful in practical applications.

The 3D patterns of critical disturbances (corresponding to the three-dimensional perturbation) are plotted in Figs. 9 and 10 to acquire additional information about the location of the stable or unstable vortices inside the flow field, where the instability may have evolved. Contours of the perturbed velocity field are displayed for viscosity ratio $r = 0.8$ and $r = 1.2$, with both ACW (Fig. 9) and CW (Fig. 10) rotations at a particular time. We note that for $r < 1$, the cases corresponding to CW rotation are more unstable than ACW cases ($\omega_{i,\mathrm{CW}} > \omega_{i,\mathrm{ACW}}$) and the reverse is true if $r > 1$.

In Figs. 9 and 10, the right panel shows the 2D view of the perturbation velocity contours. In the left panel of the figures, we have represented three slices of the flow field at the location $z = 0$,

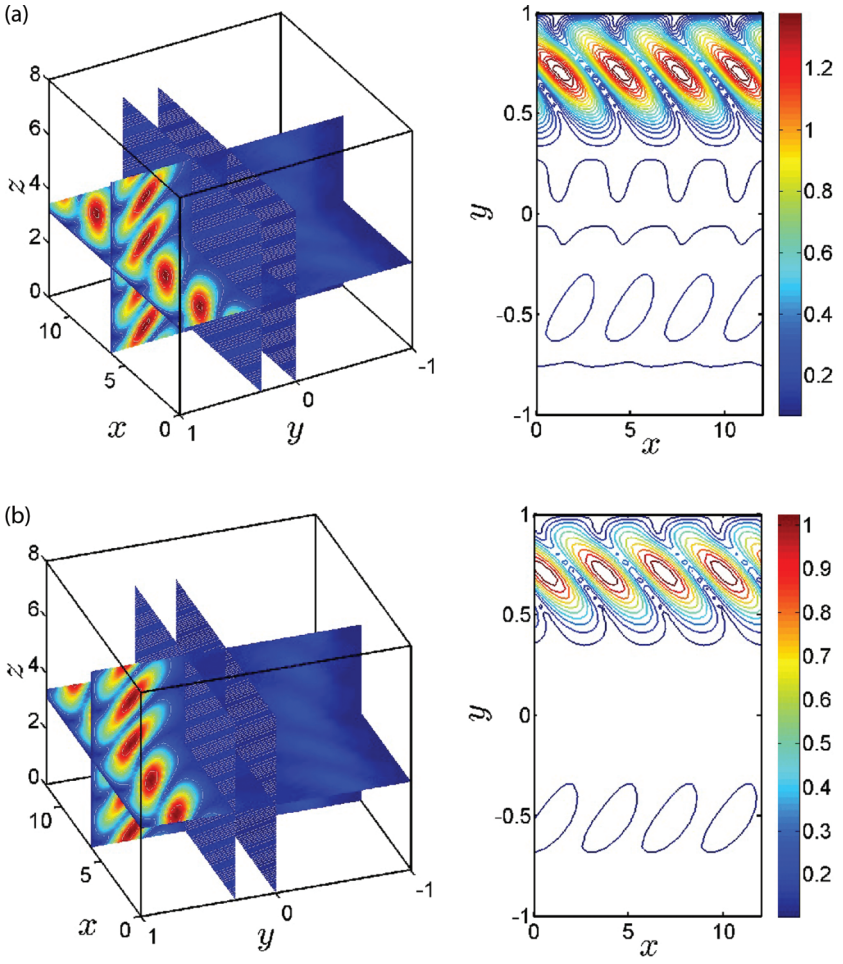

FIG. 10. Isocontours of velocity field for three-dimensional disturbances with viscosity ratio (a) $r = 1.2$ and (b) $r = 0.8$ (CWcase : Ro $= 0.2$, Re $=$ 995, $\alpha = 0.15, \beta = 1.0$). The thickness of the miscible layer $q = 0.3$ and miscible layer starts at $p = 0.0$.

$y = 0$, and $y = 0.3$ (near the mixed layer). For ACW rotation, primary vortices (with more strength) are formed in the lower layer. For $r = 0.8$, vortices are slightly stronger than that for $r = 1.2$ and the flow system with less viscous fluid adjacent to the upper wall is more unstable. Besides, for both kinds of viscosity contrasts, comparatively weaker secondary vortices are built up in the upper fluid layer of the channel. For viscosity ratio $r = 1.2$, weaker vortices are concentrated toward the midplane of the channel, dragging the disturbances inside mixed layer toward upper half (i.e., toward higher viscous liquid) from the centerline of the channel. For $r = 0.8$, similar vortices are concentrated much closer to the upper wall of the channel and hence the penetration is less in the mixed layer.

Reversing the direction of rotation (i.e., for CW case), the location of primary vortices is shifted to the upper fluid layer (which is the more viscous fluid for $r = 1.2$ and less viscous fluid for $r = 0.8$). However, secondary vortices are present in the lower layer as well. Figure 10(a) confirms that the mixed layer is more involved in the instability mechanism for $r = 1.2$. For both the viscosity ratios considered above, the secondary vortices form near $y = -0.5$, but the strength of the vortices is comparatively lower for $r = 0.8$. We also note that for the ACW rotation, the axis of the vortex

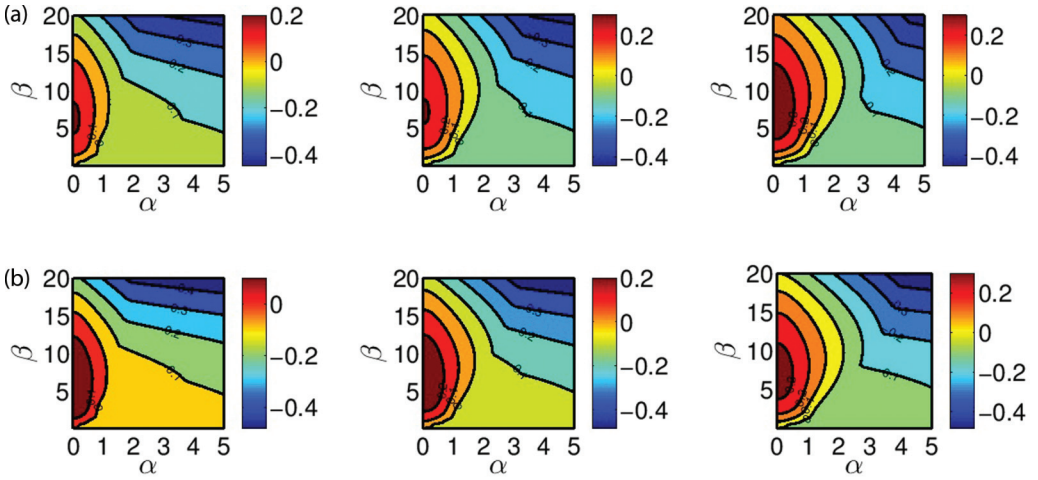

FIG. 11. Contours of maximum growth rate for (a) ACW and (b) CW rotation for three different rotation numbers Ro = 0.1, 0.2, 0.3. Other parameters are Re = 995.0, $p = 0.0$, and $q = 0.3$.

formed due to the rotation makes an acute angle with the mean flow direction, and for CW case the same makes an obtuse angle with the mean flow direction. This phenomenon might have played an eminent role in the instability mechanism.

Next, we focus our attention on the contours of the maximum growth rate ($\omega_{i,\max}$) corresponding to the 3D disturbances by considering the most unstable mode over all possible unstable streamwise and spanwise wave number. The rotation number and viscosity stratification have distinguishable effect on the critical Reynolds number. Earlier work of Alfredsson and Persson showed that for single phase flow with a spanwise system of rotation can destabilize at very low Reynolds number, and the subsequent work of Sengupta confirms the same using temporal stability theory [47,52]. Indeed, viscosity stratification influences the critical rotation number differently, which also depends on the direction of rotation. This dependence on the rotational direction comes because of the fact that the base flow becomes asymmetric due to viscosity stratification, unlike the classical plane Poiseuille flow profile which is symmetric about the central line. In Fig. 11,we tried to compare the variation of maximum growth rate for 3D disturbance on small viscosity stratified flow ($r = 1.2$) at various rotation numbers, for both ACW and CW rotation. The growth rate for ACW rotation is much higher as compared to CW rotation. Also, by increasing the rotation number, the range of streamwise and spanwise wave number for which the flow tends to become more unstable increases. The flow under 3D disturbances becomes comparatively more unstable for shorter streamwise wave numbers (longer wavelength). As we know, the order of magnitude of growth rate is always small. Thus, quantitative changes in maximum growth do not appear to be very prominent. Figure 11 is drawn at a fixed Reynolds number (Re = 995.0), since we are interested to capture the influence of rotation number on $\omega_{i,\max}$ for both ACW and CW rotation. The rotation number is varied to understand the effectiveness of the mixing process. We observe that for different rotational directions (i.e., ACW and CW rotation), the ranges of unstable streamwise and spanwise wave numbers do not vary much, but the growth rate for ACW rotation is much higher as compared to CW rotation. Also, by increasing the rotation number, the range of streamwise and spanwise wave number for which the flow tends to become more unstable increases. The flow under 3D disturbances becomes comparatively more unstable for shorter streamwise wave numbers (longer wavelength). This information is useful for designing a compact rotating device.

The earlier studies on the classical single fluid Poiseuille flow with a spanwise system of rotation showed that the base flow profile was symmetric about the central line. For standard parabolic type profile, the largest velocity is perceptible near the central line of the channel. As a result of this, the

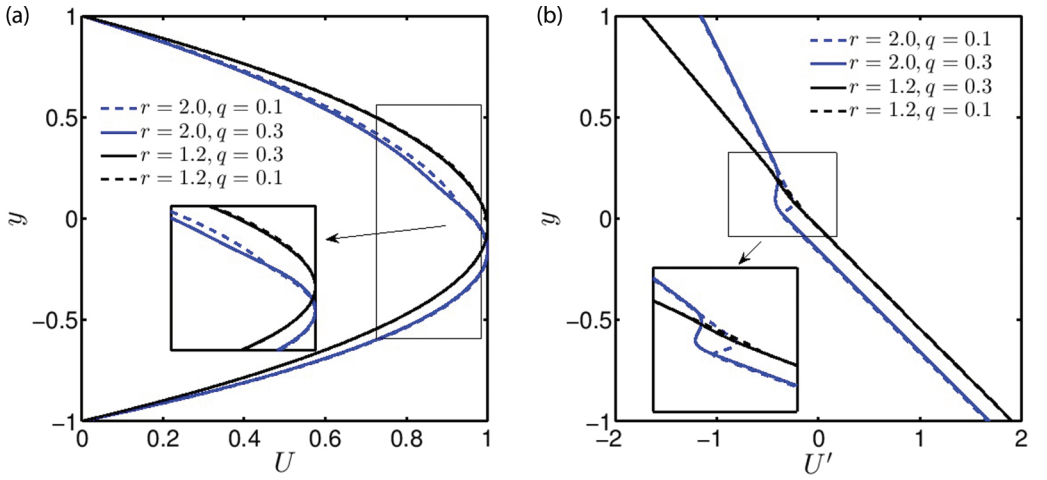

FIG. 12. (a) Base velocity profile and (b) gradient of the base flow profile for viscosity ratio $r = 1.2$, 2.0, and mixed layer starting position $p = 0.0$ with thickness $q = 0.1$ and 0.3.

Coriolis force is highly influential near the central line, leading to an unstable flow configuration and causing instability. However, altering the direction of rotation, the instability behavior does not change as the mean velocity profile is balanced about the central line. On the contrary, for the case of viscosity stratified flow, the mean velocity profile is not symmetric about the central line of the channel and the skewness of the velocity profile is completely dependent on the viscosity ratio of the fluids. The asymmetric base flow about the central line contributes to a change in instability mechanism for viscosity stratified flow system if the direction of rotation is altered. Moreover, due to the presence of the Coriolis force, the base velocity gradient plays a substantial role in modifying instability behavior.

In Fig. 12, we have plotted typical base velocity and its gradient for a viscosity stratified miscible flow with viscosity ratio $r = 2.0$. Altering the thickness of the miscible layer changes the maximum velocity, which in turn changes the range of the critical parameters (Reynolds number and Rotation number) for instability of the system due to the variation of shear rate near the mixed layer as well as centerline. It is also evident in Fig. 12(b) that the velocity gradient of the base flow may be the other possible reason due to which the flow system with the thicker miscible layer is more unstable. Furthermore, this idea is a direct consequence of Bradshaw's instability criterion [75] developed for a rotating flow system. The inclusion of the viscosity variation causes an asymmetry in the base flow which, coupled with the rotational effect, renders the system more susceptible to rotation-induced instability. It is to be noted that for a symmetrical parabolic profile, reversing the direction of rotation does not affect the neutral stability boundary. For the case of the symmetric base velocity profile, the direction of rotation does not affect the neutral stability boundary, because of the fact that the absolute value of wall normal pressure gradient from the central line is same for both ACW and CW rotations. However, with the viscosity contrast, if a fluid element is considered at the same distance above and below the central line, the absolute value of the wall normal pressure gradient no longer remains to be the same as the case of single-phase flow.

For the case of viscosity stratified miscible flow, the reported literature [3,13,18] indicates that the thinner mixed layer is more unstable for streamwise disturbances. However, our numerical findings show that viscosity stratified flow with a spanwise rotation can be more unstable for the thicker mixed layer as well. Due to the presence of spanwise rotation, the problem under investigation and associated instability mechanism are in contrast to earlier investigations dealing with viscosity stratified miscible channel flow. Here, we are investigating the instability mechanism that deals with spanwise disturbances in a rotating platform, which is different from the earlier works with

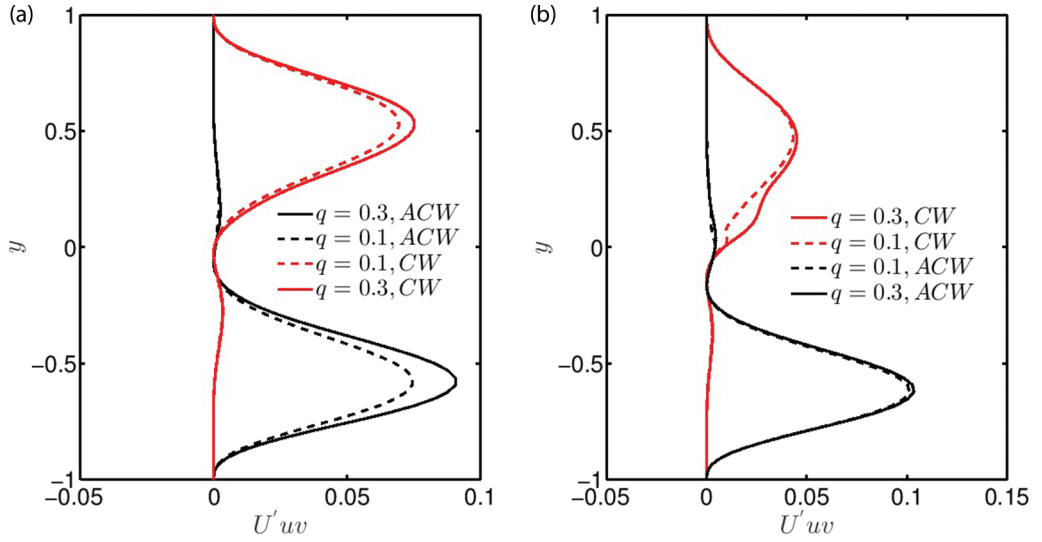

FIG. 13. Variation of the energy transfer term for viscosity ratio (a) $r = 1.2$ and for (b) 2.0. The other parameters are the critical values as mentioned in Table I. The Reynolds number and rotation number considered for the flow is Re = 995.0 and Ro = 0.2, respectively.

streamwise disturbances for the viscosity stratified flows. We have observed (see Fig. 4) that the system with thick mixed layer is more unstable, which is mainly because of the critical role of spanwise perorations as well as Coriolis effects. To understand the underlying principle behind this contradiction, we have tried to show the energy variation of the perturbed system represented by the Reynolds stress term $(U'uv)(u, v$ are the perturbation velocity components and U' is gradient of the base flow profile), drawn from base flow to transfer disturbed flow. The same is plotted as a function of y for two different miscible layer thicknesses ($q = 0.1$ and 0.3) with both ACW and CW rotation, as shown in Fig. 13. We consider the case $r > 1$ with two different viscosity ratios: $r = 1.2$ in Fig. 13(a) and 2.0 in Fig. 13(b). For both the cases, we see the thick miscible layer draws energy more efficiently from the mean flow as compared to thin miscible layer, which can cause the flow to be more unstable for a spanwise system of rotation. Altering the rotational direction, the qualitative behavior did not change. Moreover, to get the precise physical mechanism, a further critical investigation using full kinetic energy budget calculation is required.

IV. CONCLUSIONS

We have discussed the effects of instability mechanism due to Coriolis force on rotating laminar miscible viscosity-stratified two-fluid channel flows. The linear instability analysis has been conducted to explore the possible mechanisms of the system under investigation (in the context of two- and three-dimensional perturbations). The influence of viscosity ratio and thin diffusive layer (called a mixed layer) between the two fluids is taken into consideration. We have discussed the significance of frozen mixed layer thickness (q) and asymmetric base flow profile. Modal stability analysis of the flow ascertains the variation of instability mechanism for the rotating viscosity stratified flow, depending on the rotational direction. Numerical results pinpoint the following critical parameters, namely, rotation number, Reynolds number, the direction of rotation, viscosity ratio, and thickness of the miscible layer.

In contrast to the general nonrotating class of viscosity stratified flows, our analysis indicates that in the presence of spanwise disturbances, the rotating stratified flow with the thicker miscible layer is more unstable than that of the flow with thinner mixed layer. This is the most important and

novel finding of the current work. Assessment of maximum growth rate over a range of spanwise wave numbers has been conducted for different rotation numbers (for both ACW and CW rotation), to understand the efficiency of the mixing process. It has been found that the growth rate for ACW rotation is more prominent compared to CW rotation and it increases significantly on increasing the rotation number (for viscosity ratio greater than unity). We have also tried to elucidate the three-dimensional perturbed flow field qualitatively and explained how both clockwise and anticlockwise rotation can affect the flow vortices, to control the mixing process. An eigen spectrum analysis reveals that for three-dimensional disturbances, unstable modes sourcing from different layers can play a monumental role in the temporal instability, depending on the viscosity ratio (r) of the fluids. Our results demonstrate the existence of several unstable modes, some of which originate from the mixed layer. The appearance of the unstable modes from different layers relies on rotational direction and spanwise disturbances. The origin of the most unstable mode depends on the viscosity ratio, direction of rotation, and mixed layer thickness. The instability mechanisms are the outcomes of the change in maximum velocity as well as the shear rate, by virtue of the viscosity stratification. The dispersion of energy transport, as a function of wall normal direction, suggests that the flow with a thick miscible layer draws energy more efficiently from the mean flow, which may be implicitly causing the flow to be more unstable than that of the flow with thin mixed layer, in the presence of spanwise system rotation.

ACKNOWLEDGMENTS

S.C. acknowledges Department of Science and Technology, Government of India, for providing financial support by means of the J. C. Bose National Fellowship, for executing this research. S.G. gratefully acknowledges the financial support from SERB-DST, India through CRG project (Grant No. CRG/2018/004521). All the authors are thankful to the reviewers for their careful reading of the reported work and valuable suggestions to improve the quality of the paper.

APPENDIX A: NONDIMENSIONALIZATION WITH AVERAGE VELOCITY AND VISCOSITY

We define the Reynolds and rotation numbers using average velocity and average viscosity. We calculate the flow rate across the channel and thereby obtain the average velocity (tabulated below), to make the comparison between two different scalings. In Fig. 14 below, we show the critical rotation number for both, clockwise (CW) and anticlockwise (ACW) rotation for two different viscosity ratios $r = 1.2$ [Figs. 14(a) and 14(b)] and 2.0 [Figs. 14(c) and 14(d)] for layer thickness, $q = 0.3$. Comparing the results obtained in the case of using maximum velocity with that of the average velocity, one can clearly see that, with average velocity the critical rotation number increases substantially while the critical value of Reynolds number decreases. Average velocity for viscosity stratified flow is considerably less than maximum velocity (see Table II), and hence an increase in critical rotation number is evident and similarly, the critical value of Reynolds number is found to decrease. However, the qualitative results are unaltered for the scaling alteration. The critical value of rotation numbers obtained after nondimensionalizing with average velocity for viscosity ratio 1.2 are 0.53, 0.45 and viscosity ratio 2.0 are 0.43 and 0.31 for ACW and CW rotation, respectively. The critical value of Reynolds number thus can be calculated as 50.8511 (ACW) and 53.72 (CW) for viscosity ratio of 1.2 and 72.26 (ACW) and 88.23 (CW) for viscosity ratio of 2.0.

The comparison holds up against the redefinition of Reynolds number and rotation number while using the average velocity for the purpose of nondimensionalization (see Fig. 15). We find that the thicker mixed layer is less stable than the thinner layer similar to the case of scaling with maximum velocity. The used rotation number is $\mathrm{Ro} = 0.20$, which is arbitrary. However, altering the rotation number does not make any difference in the main finding under the scrutiny. Moreover, the active reason of instability due to system of rotation comes from the celebrated Bradshaw-Richardson criterion and subsequently by Pedley, which shows that the gradient Richardson number, $B^* = \mathrm{Ro}(\mathrm{Ro} - U') < 0$, determines the stability for inviscid flows in a rotating platform [75,76]. It is

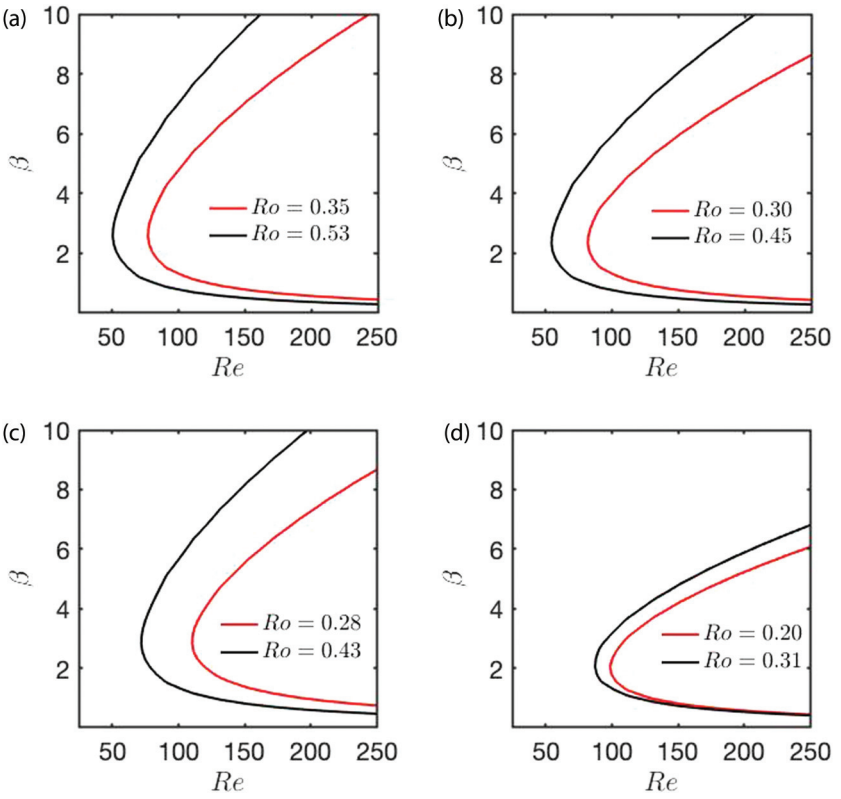

FIG. 14. Neutral stability boundaries for two different viscosity ratios (r): in (a) and (b) panels $r = 1.2$ and in (c) and (d) panels $r = 2.0$. Right and left columns of the figure are for clockwise and anticlockwise rotation, respectively. Black line represents the results using average velocity and red line represents with maximum velocity.

noticed that this criterion is also holds good for viscous flows and used by previous researchers to justify mechanism behind the rotating instability [47,51,52]. For low contrast in viscosity ($r = 1.2$), the effect of mixing layer thickness does not have much influence in the gradient of the flow field and hence the effect seems to be less on stability boundary, as it can clearly be seen from the Fig. 15(a). However, for higher viscosity contrast $r = 2.0$, the effect is more prominent and dependent on direction of rotation [see Fig. 15(b)].

To compare our results with the unstratified flow, in Fig. 16 we have shown the neutral stability boundaries for both unstratified flow and stratified flow using average velocity as the velocity scale, half channel width and averaged viscosity as length and viscosity scales, respectively. Our results

TABLE II. The flow rate, average velocity, and maximum velocity for two different viscosity ratio $r = 1.2$ and 2.0 for two different layer thickness $q = 0.1$ and 0.3.

Viscosity ratio (r)	Layer thickness (q)	Flow rate ($Q = \int_{-1}^{1} U dy$)	Average velocity ($U_{\text{avg}} = Q/\text{Area}$)	Maximum velocity (U_0)
1.2	0.1	1.214561261317564	0.607280630658782	0.911758430789031
1.2	0.3	1.215441161666708	0.607720580833354	0.914320133640885
2.0	0.1	0.918078102497246	0.459039051248623	0.698888613552727
2.0	0.3	0.924123447303222	0.462061723651611	0.711049559571532

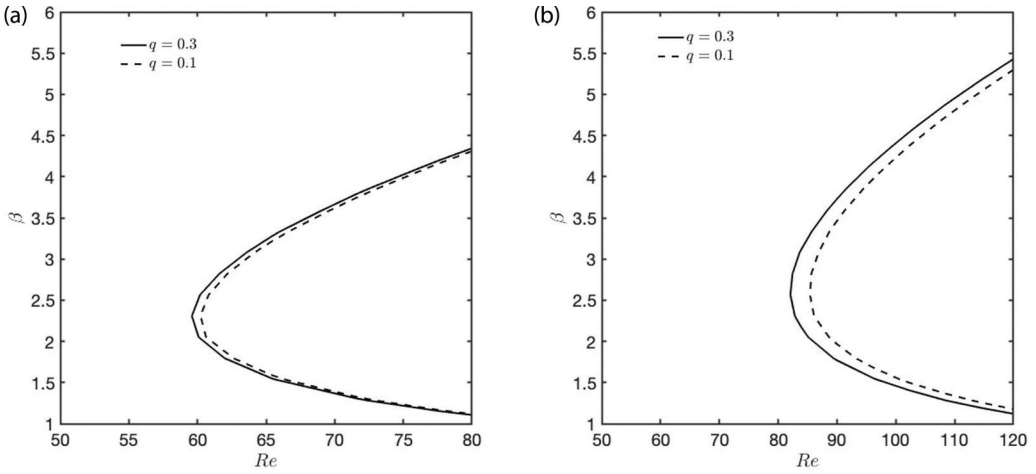

FIG. 15. The effect of layer thickness on neutral stability boundary for viscosity ratio (a) 1.2 and (b) 2.0. The other parameters are Ro = 0.20 (ACW), $q = 0.3$, and $p = 0.0$. Here, Re and Ro are defined using average velocity over the channel.

show that for unstratified case, the critical Reynolds number for the flow for both streamwise wave number $\alpha = 0.0, 1.0$ is more critical than for the viscosity stratified flow, which suggests that the viscosity stratification indeed delays the transition.

APPENDIX B: CONVERGENCE OF NUMERICAL TECHNIQUE

The numerical technique we have implemented to develop the code and thereby to solve the present problem is based on the code made available publicly by Schmid and Henningson [71] for plane Poiseuille flow. The codes described in their book have been easily available and modified

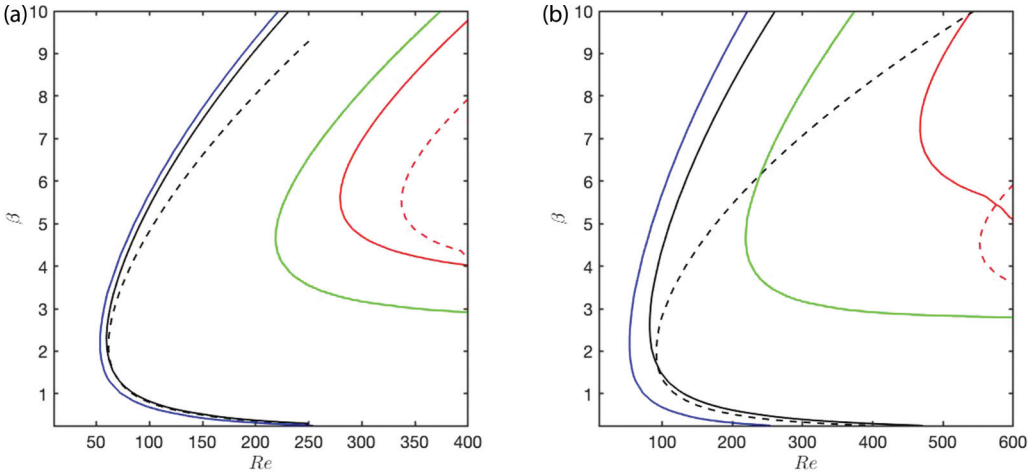

FIG. 16. Comparison with unstratified flow for viscosity ratio (r) (a) 1.2 and (b) 2.0. The blue and green line denotes unstratified flow for streamwise wave number $\alpha = 0.0, 1.0$. Dashed line represents CW rotation and solid line represents ACW rotation. Black and red line corresponds to viscosity stratified flow with streamwise wave number $\alpha = 0.0, 1.0$.

TABLE III. Convergence of nemurical value for different grid resolution, where *nu*, *nm*, and *nl* denote number of grid points in upper, miscible, and lower layer, respectively, and the comparison made with the plane Poiseuille flow results of Schmid and Henningson.

nu	*nm*	*nl*	Our computation for the considered flow	Schmid and Henningson [71] (for Poiseuille flow)
40	20	40	$0.312100195738000 - 0.019798759449700i$	$0.31210030 - 0.01979866i$
40	30	40	$0.312100475312100 - 0.019798693988600i$	
50	20	50	$0.312100426726000 - 0.019798719348000i$	
50	30	50	$0.312100706095000 - 0.019798950346000i$	
60	20	60	$0.312100129003000 - 0.019799408226000i$	
60	30	60	$0.312098328219000 - 0.019799465495000i$	

for the past 10–20 years and applied widely. We have also adhered to the same, with appropriate benchmarking.

(a) We have shown the eigen structure for viscosity ratio $r = 0.8$ and 1.2 (see Fig. 5) for both ACW and CW rotation, which has been done carefully by implimenting appropiate boundary conditions [Eqs. (13)–(25)] originating from the fact that continuity of velocity, tangential, and normal stress is maintained across interfaces of each layers.

(b) The validations are done based on three layer grid structure. A tabulated form is given herein (Table III), for the case where the grid resolution has been changed with the benchmarked data available on the the book of Schmid and Henningson for classical plane Poiseuille flow for Reynolds number $\mathrm{Re} = 2000$, $\alpha = 1.0$, $\beta = 0.0$.

APPENDIX C: USE OF SQUIRE TRANSFORMATION

The main reason of doing Squire transformation is that, failing to do so, it is impossible to incorporate the Coriolis effect in the platform of OS system. This technique of using Squire transformation for the case of rotating channel flow system has been validated by many previous research groups including ours for single phase flow [47,52,68,69]. Incorporating viscosity as a function of concentration will give rise to an additional equation [2,10,11,30], but to investigate the role played by Coriolis force on stability of such flows, a Squire transformation is always required and it has no connection with the concentration equation.

[1] Peter R. N. Childs, *Rotating Flow* (Elsevier, Amsterdam, 2011).
[2] R. Govindarajan and K. C. Sahu, Instabilities in viscosity-stratified flow, Annu. Rev. Fluid Mech. **46**, 331 (2014).
[3] S. Ghosh, R. Usha, and K. C. Sahu, Linear stability analysis of miscible two-fluid flow in a channel with velocity slip at the walls, Phys. Fluids **26**, 014107 (2014).
[4] C. E. Hickox, Instability due to viscosity and density stratification in axisymmetric pipe flow, Phys. Fluids **14**, 251 (1971).
[5] K. S. Gage and W. H. Reid, The stability of thermally stratified plane Poiseuille flow, J. Fluid Mech. **33**, 21 (1968).
[6] G. N. Ivey, K. B. Winters, and J. R. Koseff, Density stratification, turbulence, but how much mixing? Annu. Rev. Fluid Mech. **40**, 169 (2008).
[7] B. Khomami, Interfacial stability and deformation of two stratified power law fluids in plane Poiseuille flow Part I. Stability analysis, J. Nonnewton. Fluid Mech. **36**, 289 (1990).

[8] B. Khomami, Interfacial stability and deformation of two stratified power law fluids in plane Poiseuille flow Part II. Interface deformation, J. Nonnewton. Fluid Mech. **37**, 19 (1990).
[9] C.-S. Yih, Stability of liquid flow down an incline, Plane Phys. Fluids **6**, 321 (1963).
[10] C.-H. Li, Stability of two superposed elasticoviscous liquids in plane Couette flow, Phys. Fluids **12**, 531 (1969).
[11] M. Ahrens, Y. J. Yoo, and D. D. Joseph, Hyperbolicity and change of type in the flow viscoelastic fluids through pipes, J. Nonnewton. Fluid Mech. **24**, 67 (1987).
[12] A. P. Hooper and W. G. C. Boyd, Shear-flow instability at the interface between two viscous fluids, J. Fluid Mech. **128**, 507 (1983).
[13] S. V. Malik and A. P. Hooper, Linear stability and energy growth of viscosity stratified flows, Phys. Fluids **17**, 024101 (2005).
[14] F. Charru and J. Fabre, Long waves at the interface between two viscous fluids, Phys. Fluids **6**, 1223 (1994).
[15] B. T. Ranganathan and R. Govindarajan, Stabilization and destabilization of channel flow by location of viscosity-stratified fluid layer, Phys. Fluids **13**, 1 (2001).
[16] M. J. South and A. P. Hooper, Linear growth in two-fluid plane Poiseuille flow, J. Fluid Mech. **381**, 121 (1999).
[17] D. P. Wall and S. K. Wilson, The linear stability of channel flow of fluid with temperature-dependent viscosity, J. Fluid Mech. **323**, 107 (1996).
[18] R. Govindarajan, Effect of miscibility on the linear instability of two-fluid channel flow, Int. J. Multiph. Flow **30**, 1177 (2004).
[19] A. D. D. Craik and F. I. P. Smith, The stability of free-surface flows with viscosity stratification, J. Fluid Mech. **34**, 393 (1968).
[20] S. Kalliadasis, A. Kiyashko, and E. A. Demekhin, Marangoni instability of a thin liquid film heated from below by a local heat source, J. Fluid Mech. **475**, 377 (2003).
[21] J. Hu, H. Ben Hadid, D. Henry, and A. Mojtabi, Linear temporal and spatiotemporal stability analysis of a binary liquid film flowing down an inclined uniformly heated plate, J. Fluid Mech. **599**, 269 (2008).
[22] H. Goyal, A. Ananth Praveen Kumar, D. Bandyopadhyay, R. Usha, and T. Banerjee, Instabilities of a confined two-layer flow on a porous medium: An Orr–Sommerfeld analysis, Chem. Eng. Sci. **97**, 109 (2013).
[23] R. Usha, O. Tammisola, and R. Govindarajan, Linear stability of miscible two-fluid flow down an incline, Phys. Fluids **25**, 104102 (2013).
[24] S. Ghosh and R. Usha, Stability of viscosity stratified flows down an incline: Role of miscibility and wall slip, Phys. Fluids **28**, 104101 (2016).
[25] H. Wilson and J. M. Rallison, Instability of channel flows of elastic liquids having continuously stratified properties, J. Nonnewton. Fluid Mech. **85**, 273 (1999).
[26] K. C. Sahu and O. K. Matar, Stability of plane channel flow with viscous heating, J. Fluids Eng. **132**, 011202 (2010).
[27] J. J. Wyle and H. Huang, Extensional flows with viscous heating, J. Fluid Mech. **571**, 359 (2007).
[28] P. C. Sukanek, C. A. Goldstein, and R. L. Laurence, The stability of plane Couette flow with viscous heating, J. Fluid Mech. **57**, 651 (1973).
[29] C. Yueh and C. Weng, Linear stability analysis of plane Couette flow with viscous heating, Phys. Fluids **8**, 1802 (1996).
[30] C. T. Tan and G. M. Homsy, Stability of miscible displacements in porous media: Rectilinear flow, Phys. Fluids **29**, 3549 (1986).
[31] C. T. Tan and G. M. Homsy, Stability of miscible displacements in porous media: Radial source flow, Phys. Fluids **30**, 1239 (1987).
[32] J.-C. Bacri, D. Salin, and R. Wouméni, Three-Dimensional Miscible Viscous Fingering in Porous Media, Phys. Rev. Lett. **67**, 2005 (1991).
[33] P. Ern, F. Charru, and P. Luchini, Stability analysis of a shear flow with strongly stratified viscosity, J. Fluid Mech. **496**, 295 (2003).

[34] K. C. Sahu, H. Ding, P. Valluri, and O. K. Matar, Linear stability analysis and numerical simulation of miscible two-layer channel flow, Phys. Fluids **21**, 042104 (2009).
[35] B. Selvam, S. Merk, R. Govindarajan, and E. Meiburg, Stability of miscible core-annular flows with viscosity stratification, J. Fluid Mech. **592**, 23 (2007).
[36] L. Talon and E. Meiburg, Plane Poiseuille flow of miscible layers with different viscosities: Instabilities in the Stokes flow regime, J. Fluid Mech. **686**, 484 (2011).
[37] H. Li, T. N. Wong, and N.-T. Nguyen, Instability of pressure driven viscous fluid streams in a microchannel under a normal electric field, Int. J. Heat Mass Transf. **55**, 6994 (2012).
[38] M. H. Oddy, J. G. Santiago, and J. C. Mikkelsen, Electrokinetic instability micromixing, Anal. Chem. **73**, 5822 (2001).
[39] A. O. El Moctar, N. Aubry, and J. Batton, Electro-hydrodynamic microfluidic mixer, Lab Chip **3**, 273 (2003).
[40] C. Tsouris, C. T. Culbertson, D. W. DePaoli, S. C. Jacobson, V. F. de Almeida, and J. M. Ramsey, Electrohydrodynamic mixing in microchannels, AIChE J. **49**, 2181 (2003).
[41] X.-Y. You, L.-D. Zhang, and J.-R. Zheng, The stability of finite miscible liquid-liquid stratified microchannel flow with boundary slip, J. Mech. **30**, 103 (2014).
[42] X. Hu and T. Cubaud, Inertial destabilization of highly viscous microfluidic stratifications, Phys. Rev. Fluids **1**, 044101 (2016).
[43] T. Cubaud and T. G. Mason, Formation of miscible fluid microstructures by hydrodynamic focusing in plane geometries, Phys. Rev. E **78**, 056308 (2008).
[44] O. Strohmeier, M. Keller, F. Schwemmer, S. Zehnle, D. Mark, F. von Stetten, R. Zengerle, and N. Paust, Centrifugal microfluidic platforms: Advanced unit operations and applications, Chem. Soc. Rev. **44**, 6187 (2015).
[45] N. R. Glass, R. J. Shilton, P. P. Y. Chan, J. R. Friend, and L. Y. Yeo, Miniaturized Lab-on-a-Disc (miniLOAD), Small **8**, 1881 (2012).
[46] A.-C. Ruo, M.-H. Chang, and F. Chen, Effect of rotation on the electrohydrodynamic instability of a fluid layer with an electrical conductivity gradient, Phys. Fluids **22**, 024102 (2010).
[47] S. Sengupta, S. Ghosh, S. Saha, and S. Chakraborty, Rotational instabilities in microchannel flows, Phys. Fluids **31**, 054101 (2019).
[48] D. Chakraborty, M. Madou, and S. Chakraborty, Anomalous mixing behavior in rotationally actuated microfluidic devices, Lab Chip **11**, 2823 (2011).
[49] R. Burger, P. Reith, V. Akujobi, and J. Ducrée, Rotationally controlled magneto-hydrodynamic particle handling for bead-based microfluidic assays, Microfluid. Nanofluidics **13**, 675 (2012).
[50] R. Burger, D. Kirby, M. Glynn, C. Nwankire, M. O'Sullivan, J. Siegrist, D. Kinahan, G. Aguirre, G. Kijanka, R. A. Gorkin, and J. Ducrée, Centrifugal microfluidics for cell analysis, Curr. Opin. Chem. Biol. **16**, 409 (2012).
[51] D. K. Lezius and J. P. Johnston, Roll-cell instabilities in rotating laminar and trubulent channel flows, J. Fluid Mech. **77**, 153 (1976).
[52] P. H. Alfredsson and H. Persson, Instabilities in channel flow with system rotation, J. Fluid Mech. **202**, 543 (1989).
[53] O. J. E. Matsson and P. H. Alfredsson, Curvature-and rotation-induced instabilities in channel flow, J. Fluid Mech. **210**, 537 (1990).
[54] D. Chakraborty and S. Chakraborty, Controlled microbubble generation on a compact disk, Appl. Phys. Lett. **97**, 234103 (2010).
[55] S. Tottori and S. Takeuchi, Formation of liquid rope coils in a coaxial microfluidic device, RSC Adv. **5**, 33691 (2015).
[56] D. Kiriya, R. Kawano, H. Onoe, and S. Takeuchi, Microfluidic control of the internal morphology in nanofiber-based macroscopic cables, Angew. Chemie Int. Ed. **51**, 7942 (2012).
[57] D. Kiriya, M. Ikeda, H. Onoe, M. Takinoue, H. Komatsu, Y. Shimoyama, I. Hamachi, and S. Takeuchi, Meter-long and robust supramolecular strands encapsulated in hydrogel jackets, Angew. Chemie Int. Ed. **51**, 1553 (2012).

[58] P. Garstecki, M. J. Fuerstman, H. A. Stone, and G. M. Whitesides, Formation of droplets and bubbles in a microfluidic T-junction—Scaling and mechanism of break-up, Lab Chip **6**, 437 (2006).
[59] A. Gupta, S. M. S. Murshed, and R. Kumar, Droplet formation and stability of flows in a microfluidic T-junction, Appl. Phys. Lett. **94**, 164107 (2009).
[60] J. Ducrée, S. Haeberle, S. Lutz, S. Pausch, F. von Stetten, and R. Zengerle, The centrifugal microfluidic Bio-Disk platform, J. Micromech. Microengineer. **17**, S103 (2007).
[61] S. Hugo, K. Land, M. Madou, and H. Kido, A centrifugal microfluidic platform for point-of-care diagnostic applications, S. Afr. J. Sci. **110**, 1 (2014).
[62] F. Schuler, F. Schwemmer, M. Trotter, S. Wadle, R. Zengerle, F. von Stetten, and N. Paust, Centrifugal step emulsification applied for absolute quantification of nucleic acids by digital droplet RPA, Lab Chip **15**, 2759 (2015).
[63] S. Kar, S. Joshi, K. Chaudhary, T. K. Maiti, and S. Chakraborty, Generation of droplets to serpentine threads on a rotating compact-disk platform, Appl. Phys. Lett. **107**, 244101 (2015).
[64] S. Kar, U. Ghosh, T. K. Maiti, and S. Chakraborty, Haemoglobin content modulated deformation dynamics of red blood cells on a compact disc, Lab Chip **15**, 4571 (2015).
[65] P. Roy, N. K. Anand, and D. Banerjee, Numerical simulation of flow and heat transfer in radially rotating microchannels, Microfluid. Nanofluidics **15**, 397 (2013).
[66] Z. Yang and Y. C. Yortsos, Asymptotic solutions of miscible displacements in geometries of large aspect ratio, Phys. Fluids **9**, 286 (1997).
[67] K. C. Sahu and R. Govindarajan, Linear stability analysis and direct numerical simulation of two-layer channel flow, J. Fluid Mech. **798**, 889 (2016).
[68] S. Wallin, O. Grundestam, and A. V. Johansson, Laminarization mechanisms and extreme-amplitude states in rapidly rotating plane channel flow, J. Fluid Mech. **730**, 193 (2013).
[69] D. P. Wall and M. Nagata, Nonlinear secondary flow through a rotating channel, J. Fluid Mech. **564**, 25 (2006).
[70] P. G. Drazin and W. H. Reid, *Hydrodynamic Stability* (Cambridge University Press, Cambridge, 2004).
[71] P. J. Schmid and D. S. Henningson, *Stability and Transition in Shear Flows* (Springer, New York, 2001).
[72] C. Canuto, M. Y. Hussaini, A. Quarteroni, and T. A. Zang, *Spectral Methods in Fluid Dynamics* (Springer, Berlin, 1988).
[73] S. A. Orszag, Accurate solution of the Orr–Sommerfeld stability equation, J. Fluid Mech. **50**, 689 (1971).
[74] D. J. Tritton and P. A. Davies, Instabilities in geophysical fluid dynamics, in *Hydrodynamic Instabilities and the Transition to Turbulence*, Topics in Applied Physics, edited by H. L. Swinney and J. P. Gollub, Vol 45. (Springer, Berlin, Heidelberg, 1985).
[75] P. Bradshaw, The analogy between streamline curvature and buoyancy in turbulent shear flow, J. Fluid Mech. **36**, 177 (1969).
[76] T. J. Pedley, On the instability of viscous flow in a rapidly rotating pipe, J. Fluid Mech. **35**, 97 (1969).